Assessment of C, N and Si isotope tracers associated to past ocean productivity

J. R. Farmer[1,2*], J. E. Hertzberg[3*], D. Cardinal[4], S. Fietz[5], K. Hendry[6], S. L. Jaccard[7,8], A. Paytan[9], P. A. Rafter[10], H. Ren[11], C. J. Somes[12], J. N. Sutton[13], and GEOTRACES-PAGES Biological Productivity Working Group Members[14]

[1]Department of Geosciences, Princeton University, Princeton, NJ, USA

[2]Max-Planck Institute for Chemistry, Mainz, Germany

[3]Department of Ocean, Earth & Atmospheric Sciences, Old Dominion University, Norfolk, VA, USA

[4]LOCEAN (UMR7159), Sorbonne Université, IRD, CNRS, MNHN, Paris, France

[5]Department of Earth Sciences, Stellenbosch University, Stellenbosch South Africa

[6]School of Earth Sciences, University of Bristol, Bristol, UK

[7]Institute of Geological Sciences and Oeschger Center for Climate Change Research, University of Bern, Bern, Switzerland

[8]Institute of Earth Sciences, University of Lausanne, Lausanne, Switzerland

[9]Institute of Marine Sciences, University of California, Santa Cruz, Santa Cruz, CA, USA

[10]Department of Earth System Science, University of California, Irvine, CA, USA

[11]Department of Geosciences, National Taiwan University, Taipei, Taiwan
[12]GEOMAR Helmholtz Centre for Ocean Research Kiel, 24105 Kiel, Germany

[13]Univ Brest, CNRS, IRD, Ifremer, Institut Universitaire Européen de la Mer, LEMAR, Plouzané, France

[14]A full list of working group members and their affiliations appears at the end of the manuscript

*Corresponding authors: Jesse Farmer (jesse.farmer@princeton.edu) & Jennifer Hertzberg (jennifer.hertzberg@gmail.com)

Key Points:

- Review of oceanic distribution, controlling processes, and sedimentary archives of C, N, and Si isotopes
- Late Quaternary C, N, and Si sedimentary isotope records demonstrate coupling between the biological pump and atmospheric pCO_2
- Cenozoic C, N, and Si sedimentary isotope records indicate large-scale changes in nutrient sources, concentrations, and the carbon cycle

Abstract

Biological productivity in the ocean directly influences the partitioning of carbon between the atmosphere and ocean interior, thereby controlling the distributions of many elements and their isotopes in the ocean. Through this carbon cycle feedback, changing ocean productivity has long been hypothesized as a key pathway for modulating past atmospheric carbon dioxide levels and hence global climate. To reconstruct climate impacts from temporal changes in paleoproductivity, robust proxies are needed to test the connection between past ocean productivity, nutrient biogeochemistry, ocean circulation and climate. Here we compile water column carbon (C), nitrogen (N) and silicon (Si) stable isotopes from GEOTRACES-era data in four key ocean regions to review geochemical proxies of oceanic carbon and nutrient partitioning based on the C, N, and Si isotopic composition of marine sediments. Relationships between water column isotope distributions, ocean productivity, and nutrient utilization are discussed. The potential for isotope measurements in sedimentary archives to record aspects of past ocean productivity are evaluated, along with key uncertainties and limitations associated with each proxy. Constraints on past ocean productivity, nutrient cycling and utilization during late Quaternary glacial-interglacial cycles and over the Cenozoic are examined. This review highlights opportunities for future research using multielement proxy applications and emphasizes the importance of such applications to reconstructing Cenozoic climate evolution.

Plain Language Summary

The ability of ocean phytoplankton to fix carbon—and ultimately influence the air-sea partitioning of the important greenhouse gas carbon dioxide—highlights the potential for this "primary production" to influence global climate in the past and future. To improve understanding of current and future scenarios of carbon dioxide levels, geochemists study changes in primary production over geological timescales. Here, we examine some of the geochemical tools used to reconstruct past changes, specifically testing the use of nutrient-based proxies. Because nutrients fuel phytoplankton growth, tracing past nutrient uptake records important aspects of past biological production. In addition, biological incorporation also controls stable (non-radioactive) isotopic composition, which is largely preserved in marine sedimentary archives. Here we illustrate new knowledge around main processes driving the carbon, nitrogen, and silicon isotopic distribution in the water column, processes that are popularly described as the "wheel" of ocean nutrient input, uptake, export, and recycling. We include scientific caveats and the extent of uncertainty, which are important for scientific interpretation of reconstructions. We then interpret representative geochemical reconstructions of biological production and nutrient use since the last ice age and over the last 70 million years. We use this knowledge to highlight directions for future research.

1 Introduction

Within the sunlit surface ocean, pelagic photoautotrophs ("phytoplankton") use sunlight to assimilate inorganic elements into organic material via photosynthesis. This organic material, which forms the base of the oceanic food web, is either regenerated ("recycled") to release dissolved elements within the surface ocean or exported to depth below the mixed layer. The regenerated elements from this exported organic material in the deep ocean later return to the surface ocean via upwelling and mixing. The small fraction of the remaining organic material that is not regenerated in the water column will be removed via burial in the underlying sediments. This interplay of inorganic element supply, assimilation, recycling, export and loss defines what we call the "wheel" of ocean productivity (see Sigman & Hain, 2012).

Several terms define the magnitude of different components of the ocean productivity wheel. Net Primary Production (NPP) refers to the rate of production by photoautotrophs

minus their metabolic requirements (or their respiration); it is effectively the rate at which phytoplankton produce new biomass. Net Ecosystem Production (NEP) is NPP minus the total (ecosystem) respiration. When functionally constrained to the euphotic zone, at steady state, NEP equates to export production; that is, NEP equates to the removal of organic material from the surface ocean and any addition of new nutrients from external sources (i.e., atmospheric deposition or riverine input). Here we use NEP and export production interchangeably (ignoring external sources of nutrients). Integrated over the entire ocean and on sufficiently long timescales, NEP must equal the supply of new nutrients to the surface ocean (via upwelling, mixing and external sources).

The NEP component of the ocean productivity wheel is of profound interest on centennial to multimillennial timescales of paleoclimate research, as NEP provides a mechanism by which carbon is sequestered away from the atmosphere. Carbon export from the surface ocean via NEP lowers the partial pressure of atmospheric carbon dioxide (CO_2) in the surface ocean, increasing CO_2 solubility. This "biological carbon pump" (Volk & Hoffert, 1985) acts as a sink for atmospheric CO_2 over time intervals ranging from the mixing timescale of the intermediate and deep ocean (decades to millennia) at minimum, to geologic timescales for exported carbon preserved in the sediments (millennia to millions of years). Therefore, NEP represents an essential pathway for ocean drawdown and storage of atmospheric CO_2. Through this impact on atmospheric CO_2, changing NEP is central to hypotheses considered to explain glacial-interglacial changes in atmospheric CO_2 levels and climate (Broecker, 1982; Berger et al., 1989; Paytan, 2009; Sigman et al., 2010; Hain et al., 2014; Galbraith & Jaccard, 2015; Galbraith & Skinner, 2020).

Measurable parameters that record aspects of past ocean productivity are required to test hypotheses linking ocean productivity with atmospheric CO_2 and climate. Here we review geochemical proxies based upon sedimentary isotope ratios of three abundant biologically mediated elements: carbon (C), nitrogen (N), and silicon (Si). Although sedimentary C, N, and Si isotope ratios are relatively established tools within the (paleo)oceanography community, a review of their application at this time is warranted given improved understanding of ocean element and isotopic distributions from GEOTRACES and other hydrographic surveys. A synthesis of trace elements and their isotopes as potential paleoproductivity proxies is provided in a companion manuscript (Horner et al., *this volume*).

Paleoproductivity proxies encompass a broad spectrum of tools, including proxies for sedimentary redox conditions (Tribovillard et al., 2006), flux-normalized accumulation of

organic debris within sediments (Costa et al., 2020), and nutrient tracers, the last of which is the principal focus for this manuscript. Sedimentary C, N, and Si isotopes do not measure export production directly. Instead, these tools track element utilization, that is, the ratio between element supply to the surface ocean and biological element consumption. For the case of nutrients, utilization is directly relevant to export production because the quantity of nutrient uptake equals the amount of carbon drawdown through export production at steady state (Dugdale & Goering, 1967; Eppley & Peterson, 1979). In this context, proxies for past nutrient utilization can constrain the past behavior of the biological pump, as the balance between nutrient supply and consumption links directly to the balance between ocean carbon uptake and release (Robinson et al., 2005).

However, nutrient isotope proxies face a shared weakness with respect to productivity: once element consumption progresses to completion (as is the case for N and Si in oligotrophic regions), changes in isotope ratios no longer scale with export production (Section 3, below). In these oligotrophic settings, nutrient isotope proxies still provide valuable information on processes impacting regional nutrient inputs to and losses from the ocean. Given sufficient constraints, such records can inform on changes in global nutrient inventories, with direct relevance to global ocean productivity and climate (Broecker, 1982).

In this review, we address three questions for C, N, and Si isotopes:

(1) *Which processes does the element/isotope ratio track?* How does ocean productivity impact the element/isotope ratio? Can the impact of productivity be distinguished from processes at ocean interfaces and other internal cycles?

(2) *Where can the element/isotope ratio be measured?* Are sediment archives available for reconstructing past variations in the element/isotope ratio? If so, which archive(s) hold the most promise? What are the assumptions associated with using each of these archives?

(3) *What research priorities would make the element/isotope ratio more useful for paleoproductivity studies?* Where do current uncertainties lie, and what research directions could improve the veracity of paleoproductivity reconstructions using these tools?

2 Data notations and sources

2.1 Reporting of isotope ratios

Isotope ratios are reported in δ notation, expressing the part-per-thousand (‰) deviation in sample isotope ratio relative to accepted international standards of known isotopic composition:

$$\delta^{13}C = \left(\frac{{}^{13}C / {}^{12}C_{sample}}{{}^{13}C / {}^{12}C_{VPBD}} - 1 \right) * 1000 \quad (1)$$

$$\delta^{15}N = \left(\frac{{}^{15}N / {}^{14}N_{sample}}{{}^{15}N / {}^{14}N_{airN2}} - 1 \right) * 1000 \quad (2)$$

$$\delta^{30}Si = \left(\frac{{}^{30}Si / {}^{28}Si_{sample}}{{}^{30}Si / {}^{28}Si_{NBS28}} - 1 \right) * 1000 \quad (3)$$

where VPBD, air N_2 and NBS28 are the accepted international standards for C, N, and Si isotopes, respectively.

2.2 Data sources

Seawater data presented here are sourced from four oceanographic regions of distinct hydrography, biogeochemistry and export production: The North Atlantic Subtropical Gyre (hereafter NASTG), the eastern tropical South Pacific (hereafter ETSP), the central tropical South Pacific (hereafter CTSP), and the Southern Ocean. Southern Ocean data are further subdivided into the Subantarctic Zone (hereafter SAZ), between the Subantarctic Front and the Polar Front, the Open Antarctic Zone (hereafter OAZ), between the Polar Front and the Southern Antarctic Circumpolar Front (SACCF), and the Polar Antarctic Zone (PAZ) south of the SACCF. Data were principally sourced from the GEOTRACES IDP2017 (Schlitzer et al., 2018) complemented with additional datasets to address data gaps as described below.

Carbon isotopes in dissolved inorganic carbon (DIC) were collected along GEOTRACES sections GA03 (Quay & Wu, 2015), GP16 (P. Quay, https://www.bodc.ac.uk/data/documents/nodb/502092/), and GI04 (Y. Kumamoto, https://www.bodc.ac.uk/data/documents/nodb/321702/). Nitrogen isotopes of dissolved nitrate were collected on GEOTRACES section GA03 (Marconi et al., 2015) and GP16

(Peters et al., 2018). As no Southern Ocean nitrate isotope data are available in GEOTRACES IDP2017, nitrogen isotope data of nitrate plus nitrite from GOSHIP I08S (Fripiat et al., 2019) were supplemented. Silicon isotopes in silicic acid were collected along GEOTRACES section GA03 (Brzezinski & Jones, 2015) and GIPY04 (Fripiat et al., 2012).

Available data from each region (typically representing three to ten hydrographic stations) were binned via depth, and a smoothed spline fit was generated in MATLAB with a smoothing parameter (p) of $1x10^{-4}$ to $1x10^{-6}$. The exact value of p was chosen to minimize root mean square error and depict regional-scale water column features while diminishing local variability (Fig. 1).

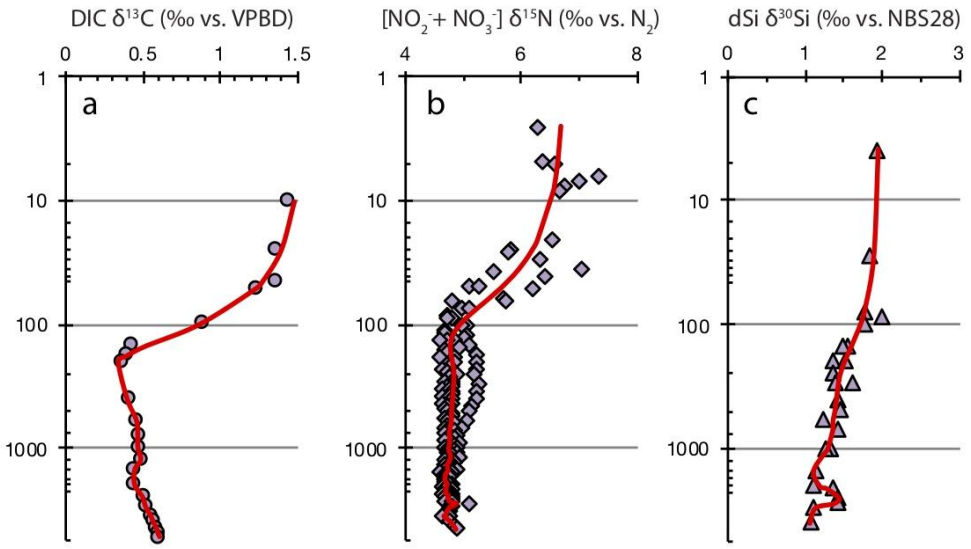

Figure 1. *Smoothed spline fits to Polar Antarctic Zone water column data for $\delta^{13}C_{DIC}$ (a, circles), $[NO_2^- + NO_3^-]$ $\delta^{15}N$ (b, diamonds), and dSi $\delta^{30}Si$ (c, triangles). Data sources: (a) GEOTRACES GI04 Station ER-14 (Y. Kumamoto), (b) GOSHIP I08S stations 5, 8, 12, 19, and 25 (Fripiat et al., 2018), (c) GEOTRACES GIPY04 stations 72 and 78 (Fripiat et al., 2012).*

3 Common processes

At steady state, the flux of nutrients driving primary production in the surface ocean will be equal to the export of these same elements out of the surface ocean. With this assumption in mind, Dugdale & Goering (1967) equated the consumption of the nutrient nitrate—the primary form of fixed nitrogen (N) delivered to the surface ocean—to the

organic matter exported from the surface ocean at steady state. Later work elaborated on this relationship, stressing that nitrate consumption in the surface ocean is:

> "quantitatively equivalent to the organic matter that can be exported from the total production in the euphotic zone without the production system running down." (Eppley & Peterson, 1979).

This observation (specific for nitrate, but translatable to C, Si, and other biologically utilized elements) provides a simple construct for paleoproductivity reconstructions: Assuming steady state, past export productivity can be reconstructed from knowledge of either the flux of the limiting nutrient into the surface ocean or flux of biogenic material out of the surface ocean. In reality, both quantities are quite challenging to ascertain from the elemental composition of marine sediments, as discussed in detail elsewhere (Berger et al., 1989; Paytan, 2009; Felix, 2014).

The isotopic composition of these major elements preserved in different sedimentary archives provides an alternative toolbox to assess past changes in nutrient supply, consumption and export production. Uptake and assimilation of elements by phytoplankton typically occurs with a preference for the lighter isotope (Fig. 2). For example, phytoplankton preferentially assimilate ^{12}C over ^{13}C by approximately 19 parts per thousand (Sackett et al., 1965; Degens et al., 1968), and ^{14}N over ^{15}N by approximately 4 to 7 parts per thousand (Waser et al., 1998; Fripiat et al., 2019). Silicifiers exhibit a similar preference for isotopically lighter dissolved silicic acid by approximately 1 part per thousand (e.g., De la Rocha et al., 1997; Sutton et al., 2013). Simple quantitative models relate the isotopic composition of nutrient supply and the degree of biological nutrient drawdown to the isotopic composition of biogenic production (Mariotti et al., 1981; Sigman & Fripiat, 2019). These models follow closed system ("Rayleigh") or open system ("steady-state") pathways:

Closed system (Rayleigh): $\delta^{i}X_{biogenic} = \delta^{i}X_{nutrient\ supply} + \varepsilon^{*}[f / (1 - f)]^{*}\ln(f)$ (4)

Open system (Steady-state): $\delta^{i}X_{biogenic} = \delta^{i}X_{nutrient\ supply} - \varepsilon^{*}f$ (5)

where for a given element X, $\delta^{i}X_{nutrient\ supply}$ is the isotopic composition of the nutrient supply, ε is the isotope effect (fractionation) expressing the isotope preference during uptake and assimilation, and f is the degree of consumption of the nutrient supply. In the Rayleigh model, the accumulated biogenic production (Eq. 4) derives from a nutrient pool that is "closed"

from resupply or loss (aside from uptake) during biogenic production. In the steady-state model, the accumulated biogenic production (Eq. 5) derives from a nutrient pool that is "open" and subject to continuous resupply.

The above models and Figure 1 highlight two consequences for paleoproductivity estimates. First, it is clear that the biological consumption of C, N, and Si, biogenic export, and remineralization (arrows inside orange box, Fig. 2) are deterministic processes for the isotopic compositions of exported biogenic production and the oceanic dissolved inorganic element inventory. Under certain conditions (discussed in detail below), mathematical models that relate the isotopic composition of biogenic material to nutrient supply and consumption (Eq. 4 and 5) can be inverted, such that isotopic measurements of biogenic material allow for reconstruction of the past degree of surface ocean nutrient consumption (*f*), which can scale with NEP under steady-state conditions. However, biological consumption, export and remineralization are not the only influences on the concentration and isotopic composition of dissolved inorganic elements. Other processes—internal and at interfaces—alter $\delta^{i}X_{nutrient\ supply}$ in Eq. 1 and 2 and can occur over a range of spatiotemporal scales (arrows outside orange box, Fig. 2). Constraining these other processes requires additional data for each element, as discussed below.

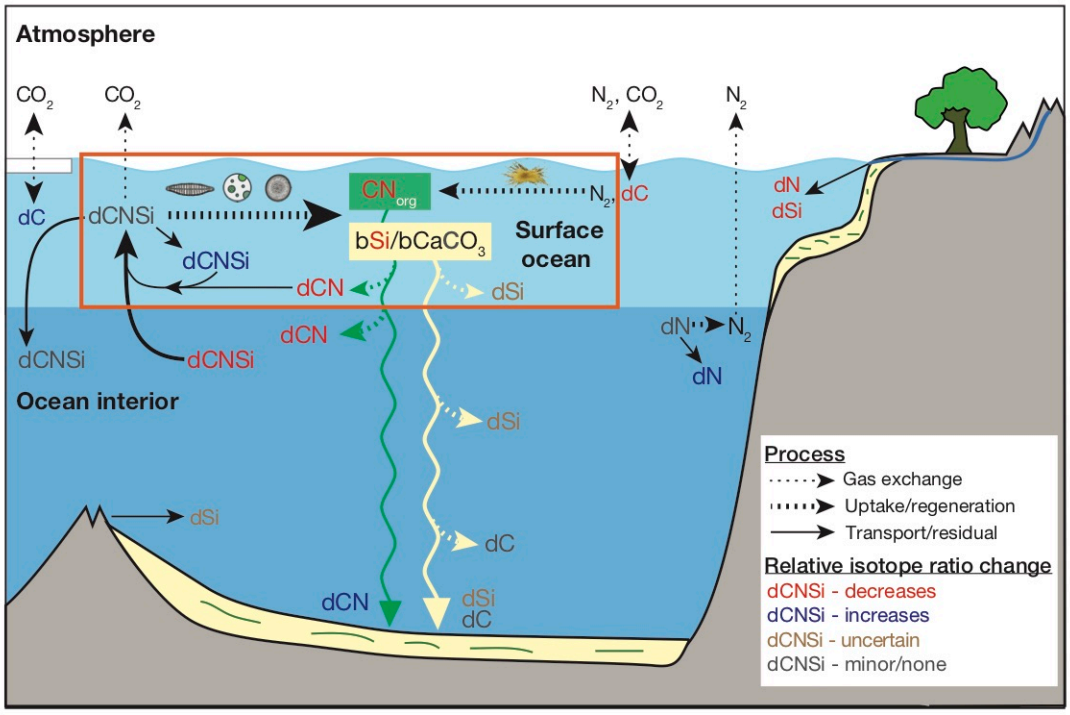

Figure 2. *Schematic summary of processes affecting isotopic composition of dissolved C, N, and Si (dCNSi). Processes related to biological productivity are outlined in the orange box. Gas exchange processes are*

indicated by dotted arrows; uptake and regeneration follow dashed arrows. Solid arrows indicate dissolved element transport due to ocean circulation or sinking, or the residual dissolved element pool resulting from incomplete consumption during uptake. Red/blue/brown/gray elements denote a relative decrease/increase/uncertain/minor change to the isotopic composition (δ-value) of the element resulting from the associated process. Basemap modified after Hain et al. (2014).

4 Carbon isotopes

Dissolved inorganic carbon (DIC) is present at abundant quantities in the oceans as aqueous carbon dioxide CO_2, bicarbonate HCO_3^-, and carbonate CO_3^{2-}. As carbon is an essential element for life, biological production consumes DIC. However, DIC consumption differs from that of nitrogen and silicon in one key fashion. Whereas nitrogen and silicon are principally supplied from the ocean interior and may be completely consumed in surface waters (Sections 5 and 6), DIC is never completely consumed in the surface ocean, reflecting both its abundant concentration and continual resupply by exchange with atmospheric CO_2 (Fig. 2).

Deviations in the abundances of the two stable isotopes of carbon (^{12}C and ^{13}C) throughout the water column reflect a combination of biological, physical, and chemical processes. Here we focus on the $\delta^{13}C$ of DIC ($\delta^{13}C_{DIC}$), which primarily reflects the $\delta^{13}C$ of bicarbonate because the DIC pool is > 90% bicarbonate at the average ocean pH of 8.1.

4.1 Modern ocean $\delta^{13}C$-DIC distribution

The general pattern of $\delta^{13}C_{DIC}$ in the modern ocean consists of higher $\delta^{13}C_{DIC}$ in the surface ocean, a subsurface minimum between 100-1000 m depth, and lower $\delta^{13}C_{DIC}$ in deeper waters (Fig. 3b). The highest $\delta^{13}C_{DIC}$ is observed in the upper 100 m of the CTSP and SO PAZ, and the lowest $\delta^{13}C_{DIC}$ overall is in the ETSP. The difference in surface ocean $\delta^{13}C_{DIC}$ between these regions is about 1‰, but the CTSP and ETSP converge to similar values below 1000 m. Of the four regions shown in Fig. 3b, the NASTG has the lowest range of $\delta^{13}C_{DIC}$ with depth. While the ETSP, CTSP, and SO PAZ all have lower $\delta^{13}C_{DIC}$ below 1000 m than in the upper 10 m, the NASTG has similar $\delta^{13}C_{DIC}$ values in the upper 10 m and

below 1000 m. The regional contrast in these patterns is due to spatial differences in the strength of driving processes and varying oceanographic regimes, as described below.

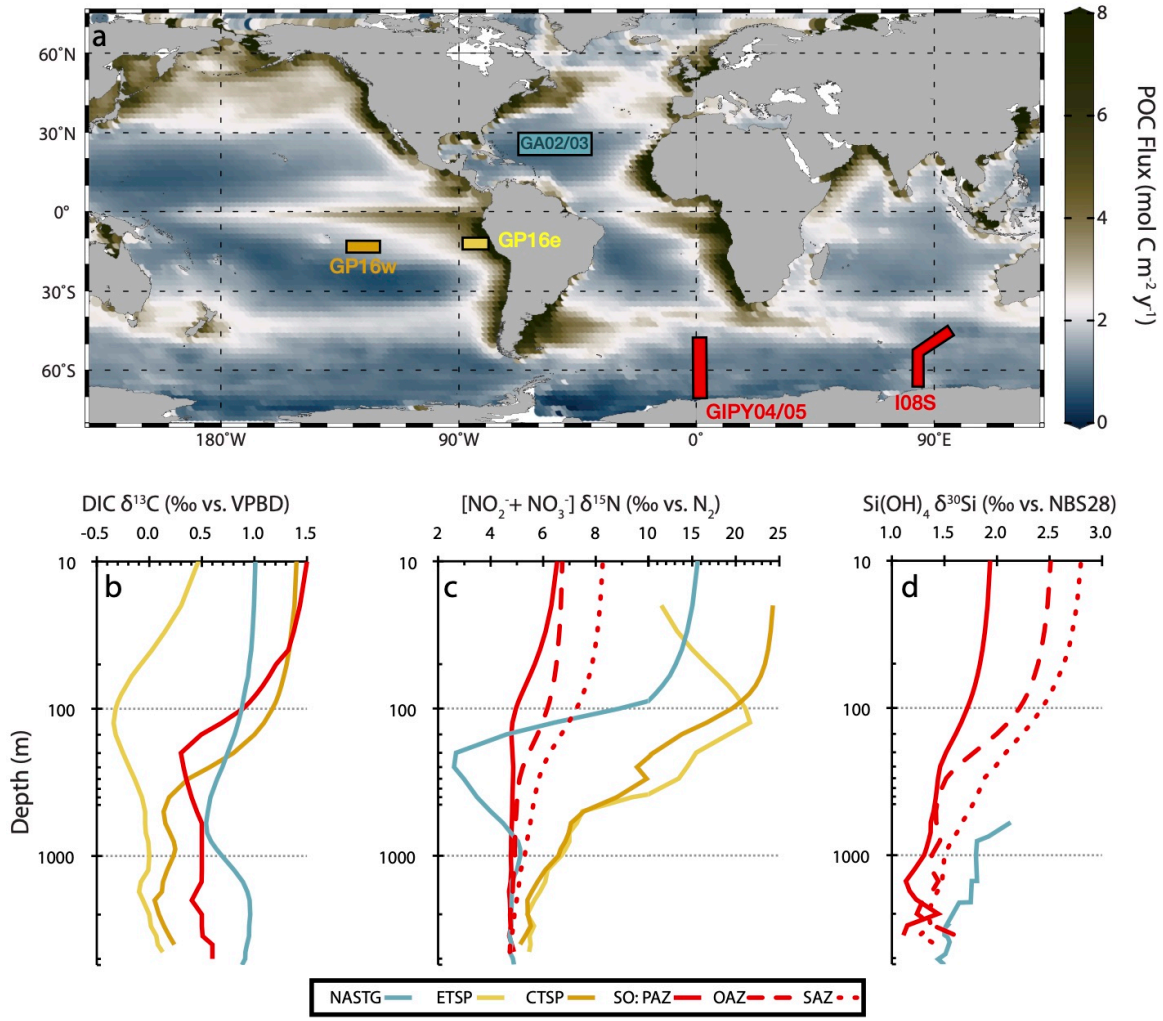

Figure 3. *Water column profiles of major element isotope ratios. a) Global data assimilation model of net export production calculated as C flux at the base of the euphotic zone (DeVries & Weber, 2017). Colored boxes denote regions and cruises of water column element concentration and isotope data. b) carbon isotopes in DIC, c) nitrogen isotopes in nitrate+nitrite, d) silicon isotopes in silicic acid versus depth. Lines are smoothed spline fits to water column data (Fig. 1). Dashed red line is from open Antarctic Zone (OAZ); dotted red line is from Subantarctic Zone (SAZ), solid red line is from the Polar Antarctic Zone (PAZ), blue line is from the NASTG (North Atlantic Subtropical Gyre), yellow line is from the ETSP (Eastern Tropical South Pacific), and brown line is from the CTSP (Central Tropical South Pacific). See Section 2.2 for data sources.*

4.2 Driving processes of modern ocean $\delta^{13}C_{DIC}$ distribution

Analyzing the distribution of $\delta^{13}C_{DIC}$ in the global oceans, Kroopnick (1974, 1985) noted that $\delta^{13}C_{DIC}$ was mainly influenced by photosynthetic kinetic fractionation and respiration in the surface waters and remineralization of organic matter in the deeper ocean. Marine phytoplankton preferentially incorporate the lighter ^{12}C during photosynthesis,

leaving the photic zone DIC relatively more enriched in ^{13}C (Fig. 2). This fractionation of about -19‰ for marine photosynthesis leaves the residual DIC in the nutrient depleted surface ocean with a high $\delta^{13}C_{DIC}$ compared to that of deep water (Lynch-Stieglitz et al., 1995). As organic matter, which is strongly enriched in ^{12}C, sinks out of the photic zone, it is subject to microbial degradation and remineralization. This process results in the release of ^{12}C enriched DIC and nutrients at depth, lowering the $\delta^{13}C_{DIC}$ of deeper waters. A decrease in the production of organic matter in the photic zone will decrease $\delta^{13}C_{DIC}$ in the surface ocean and increase $\delta^{13}C_{DIC}$ at depth, as less ^{12}C is removed from the DIC pool for photosynthesis and released at depth during remineralization (Fig. 2). Therefore, the overall pattern of $\delta^{13}C_{DIC}$ in the ocean is one of higher $\delta^{13}C_{DIC}$ in the surface ocean and lower $\delta^{13}C_{DIC}$ at depth (Fig. 3b).

A further feature of the $\delta^{13}C_{DIC}$ of deep water is the gradual increase in ^{12}C enrichment with time as a result of accumulated organic matter respiration at depth, beginning at the time a water mass is no longer in contact with the atmosphere. As a result, the $\delta^{13}C_{DIC}$ of deep waters decreases with increasing age. Following the broad pattern of global deep ocean circulation, this effect results in lower $\delta^{13}C_{DIC}$ in the deep Pacific than in the deep Atlantic at present (Fig. 3b) and makes $\delta^{13}C$ a non-conservative tracer of deep-water masses (e.g. Curry & Oppo, 2005).

In addition to biological $\delta^{13}C$ fractionation, equilibrium fractionation during air-sea gas exchange can influence the $\delta^{13}C_{DIC}$ in surface seawater (Fig. 2). If atmospheric CO_2 were in isotopic equilibrium with oceanic DIC, the DIC pool would be enriched in ^{13}C relative to atmospheric CO_2 by ~8‰ at 20 ºC (Zhang et al. 1995). During invasion of atmospheric CO_2 into surface seawater, aqueous CO_2 fractionates by -1.1‰ at 20ºC, but subsequent fractionation with respect to HCO_3^- and CO_3^{2-} results in an overall enrichment of ~8‰ (Lynch-Stieglitz et al. 1995). These equilibrium fractionations also depend on the temperature of equilibration, with surface water DIC becoming more enriched relative to atmospheric CO_2 by ~1‰ per degree of cooling (Mook et al., 1974). However, for a 50 m deep surface mixed layer, it would take ~10 years for the carbon isotopes to equilibrate between the atmosphere and ocean, which is longer than the residence time of most water masses at the ocean surface (Broecker & Peng, 1982). As a result, there is no region in the ocean where surface water $\delta^{13}C_{DIC}$ is in complete isotopic equilibrium with atmospheric $\delta^{13}C_{CO2}$ (Broecker & Maier-Reimer, 1992). In some regions, the effects of gas exchange and

biology on surface water $\delta^{13}C_{DIC}$ work together, such as the subpolar oceans where both tend to increase $\delta^{13}C_{DIC}$, while in the subtropics, biology acts to increase $\delta^{13}C_{DIC}$ but gas exchange tends to decrease $\delta^{13}C_{DIC}$ (Schmittner et al., 2013) (Fig. 2 and 3b).

Another factor that has influenced oceanic $\delta^{13}C_{DIC}$ over the industrial era is the ^{13}C "Suess" effect (Keeling, 1979). The CO_2 emitted to the atmosphere from fossil fuel combustion is strongly depleted in ^{13}C, leading to a reduction in the $\delta^{13}C$ of atmospheric CO_2. Measurements from air trapped in ice cores show that the preindustrial background $\delta^{13}C_{CO2}$ was around -6.4‰ (Bauska et al., 2015), but had declined to -8.4‰ by 2014 (Keeling et al., 2017). Air-sea exchange has resulted in the propagation of this ^{13}C Suess effect into the upper ocean, decreasing upper ocean $\delta^{13}C_{DIC}$ values (Eide et al., 2017) and weakening the $\delta^{13}C_{DIC}$ gradient between the surface and deep ocean (Olsen & Ninnemann, 2010).

4.3 $\delta^{13}C$ Archives

The use of carbon isotopes as a paleoproductivity proxy was first suggested by Tappan (1968), who noted that higher $\delta^{13}C$ values in the carbonate tests of surface dwelling planktic foraminifera were indicative of periods of increased organic carbon burial in marine sediments and possibly increased NEP. The $\delta^{13}C$ of foraminifera tests is controlled by the $\delta^{13}C_{DIC}$ of the seawater in which the calcite test precipitated. Laboratory experiments have also demonstrated that the $\delta^{13}C$ of foraminiferal calcite varies with symbiont photosynthesis, respiration, and seawater $[CO_3^{2-}]$ (Spero, 1998). The combined influence of these physiological processes shifts planktic foraminiferal $\delta^{13}C$ away from carbon isotopic equilibrium. Carbon isotope data obtained from tests collected from plankton tows or sediment traps can help determine average population or even specific species offsets from $\delta^{13}C_{DIC}$ so that the fossil record of planktic foraminiferal $\delta^{13}C$ can be used to reconstruct past $\delta^{13}C_{DIC}$ (Spero et al., 2003). The $\delta^{13}C$ of epifaunal benthic foraminifera species that live close to the sediment/water interface generally reflects the $\delta^{13}C_{DIC}$ of bottom water masses and can be used to reconstruct the $\delta^{13}C_{DIC}$ of deep waters (Woodruff et al., 1980).

The $\delta^{13}C$ difference between surface dwelling planktic and epifaunal benthic foraminifera can be used to reconstruct the vertical gradients in $\delta^{13}C_{DIC}$ between the surface and deep ocean in the past. These vertical gradients are assumed to reflect the integrated efficiency of the ocean's biological soft-tissue pump (Broecker, 1982; Shackleton et al., 1983). The larger the difference between benthic and planktic $\delta^{13}C$ (e.g., the steeper the $\delta^{13}C_{DIC}$ gradient) the higher the productivity is assumed to have been for the time period of

interest. Conversely, a smaller difference (weaker $\delta^{13}C_{DIC}$ gradient) is indicative of a weaker biological pump and decreased productivity. Because export productivity varies considerably in the ocean at any given time, samples from many sites need to be analyzed to obtain a meaningful global average. It is important to keep in mind, however, that changes in ocean circulation can modify deep water $\delta^{13}C$ independently of productivity.

Another use of foraminifera $\delta^{13}C$ relies on $\delta^{13}C$ gradients between bottom waters and sediments. While the $\delta^{13}C$ of epifaunal benthic foraminifera reflects the $\delta^{13}C_{DIC}$ of bottom water, infaunal species that calcify within the sediment pore water record a $\delta^{13}C_{DIC}$ signal dependent on bottom-water dissolved oxygen contents and organic matter fluxes (McCorkle et al., 1990). The $\delta^{13}C$ difference between epifaunal and shallow infaunal benthic foraminiferal $\delta^{13}C$ values ($\Delta\delta^{13}C_{E\text{-}I}$) has been suggested as a proxy for bottom water oxygen concetration, which may relate to productivity given that the $\delta^{13}C$ difference is proportional to the organic carbon flux to the seafloor and related remineralization rate of organic matter in the uppermost sediment layer (McCorkle et al., 1990; Hoogakker et al., 2015; Hoogakker et al., 2018).

4.4 Sources of uncertainty for paleoproductivity estimation using $\delta^{13}C$

Using $\delta^{13}C$ as a paleoproductivity proxy is not straightforward, as other processes can control $\delta^{13}C_{DIC}$ and the $\delta^{13}C$ of foraminifera. As noted earlier, changes in ocean circulation can modify deep water $\delta^{13}C_{DIC}$, and thus benthic foraminiferal $\delta^{13}C$, independently of productivity. For example, an altered Atlantic Meridional Overturning Circulation (AMOC) regime during the last glacial period resulted in a different water mass geometry in the Atlantic Basin than today that was recorded in the $\delta^{13}C$ of benthic foraminifera (e.g. Sarnthein et al., 1994; Curry & Oppo, 2005). Other processes that can modify seawater $\delta^{13}C_{DIC}$ independently of productivity include air-sea gas exchange, upwelling, and mixing of water masses with different $\delta^{13}C_{DIC}$. In addition, integrated changes are needed to examine changes in climate impacts globally, but NEP varies considerably from site to site. When reconstructing paleoproductivity from the $\delta^{13}C$ of foraminifera, species-specific fractionation effects (Spero et al., 2003) and the influence of seawater carbonate ion concentration on foraminiferal $\delta^{13}C$ (Spero et al., 1997) should be considered. For reconstructions of productivity from epifaunal-infaunal benthic $\delta^{13}C$ differences ($\Delta\delta^{13}C_{E\text{-}I}$), regeneration of organic matter in sediment depends on the oxygenation of deep water, which is also a function of circulation and temperature. The $\delta^{13}C$ of infaunal foraminifera may also be

modified by contributions of isotopically light carbon from anaerobic processes (denitrification and sulfate reduction) in sediment pore waters, which can bias oxygenation reconstructions based on the $\Delta\delta^{13}C_{E\text{-}I}$ proxy (Jacobel et al., 2020).

Applications of carbon isotopes as paleoproductivity proxies and opportunities for future research are discussed further below in Section 7.

5 Nitrogen isotopes

Bioavailable nitrogen ('fixed' from atmospheric N_2) in the ocean exists predominantly as nitrate (NO_3^-), with smaller but locally important contributions of ammonium (NH_4^+) and nitrite (NO_2^-). The supply of nitrate limits biological productivity in much of the tropical and temperate oceans. Indeed, the quantity of organic matter exported from the surface ocean (e.g., NEP) has been linked directly to the consumption of nitrate (Dugdale & Goering, 1967; Eppley & Peterson, 1979). Input and loss fluxes of fixed nitrogen are large relative to the oceanic fixed nitrogen inventory, with an estimated residence time of less than 3000 years (Brandes & Devol, 2002; Somes et al., 2013). Given the ubiquitous demand for fixed nitrogen by primary producers, nitrogen and its stable isotopes (^{15}N and ^{14}N) are powerful tracers for the degree of nitrate consumption for certain oceanographic settings and can inform on changes in marine fixed nitrogen sources and sinks in other settings.

5.1 Modern ocean nitrate $\delta^{15}N$ distribution

The $\delta^{15}N$ of nitrate broadly decreases from the surface to deep ocean in all regions (Fig. 3c). The highest $\delta^{15}N_{nitrate}$ is observed in the upper 50 m of the CTSP and NASTG, with progressively lower $\delta^{15}N_{nitrate}$ in the upper 50 m of the SAZ, OAZ and PAZ, respectively. In the ETSP oxygen deficient zone, $\delta^{15}N_{nitrate}$ increases with depth to a maximum around 120 m before progressively decreasing below 120 m. A sharp $\delta^{15}N_{nitrate}$ decrease with depth between 40 and 300 m is observed in low latitude regions. At these depths, NASTG $\delta^{15}N_{nitrate}$ is notably lower (<4‰), while ETSP and CTSP $\delta^{15}N_{nitrate}$ are higher (>8‰), than Southern Ocean $\delta^{15}N_{nitrate}$ (5-7‰). At depths below 3000 m, $\delta^{15}N_{nitrate}$ from all major ocean basins

converges on the mean deep ocean value of 5.0±0.3‰ (Sigman et al., 2000; Rafter et al., 2019).

5.2 Driving processes

Variations in $\delta^{15}N$ of nitrate (Fig. 3c) illustrate the combination of preferential assimilation of ^{14}N-nitrate to organic matter by phytoplankton in the surface ocean, regeneration of nitrate by remineralization of organic matter at depth, and varying subsurface $\delta^{15}N_{nitrate}$ arising from isotopic fractionations associated with the relative balance between regional nitrogen fixation and denitrification (Fig. 2; e.g., Somes et al., 2010; Rafter et al., 2019; Sigman & Fripiat, 2019). The $\delta^{15}N$ of organic matter exported from the surface ocean is influenced by: (1) the $\delta^{15}N_{nitrate}$ of the surface water mass, which depends on subsurface source water signatures resulting from a combination of N cycle processes including local N_2 fixation and/or denitrification, and (2) the extent of nitrate utilization (i.e. consumption relative to supply). We describe these two influences below.

First, if nitrate is not completely consumed at the surface, phytoplankton will preferentially incorporate ^{14}N nitrate (Altabet & Francois, 1994). As nitrate utilization increases, this preferential ^{14}N nitrate consumption progressively elevates the residual $\delta^{15}N_{nitrate}$ in the surface ocean relative to the subsurface nitrate supply. This fractionation during uptake explains the elevated (>10‰) $\delta^{15}N$ of residual nitrate in the upper ~100 m of the NASTG relative to the subsurface source (Marconi et al., 2015). The highest surface $\delta^{15}N_{nitrate}$ shown in Fig. 3c (>20‰) is from stations in the CTSP and is caused by an initially elevated subsurface source $\delta^{15}N_{nitrate}$ and additional fractionation during consumption while the nitrate moves away from the initial site of upwelling (Peters et al. 2018). A similar surface $\delta^{15}N_{nitrate}$ distillation occurs in the Southern Ocean, where the lowest $\delta^{15}N_{nitrate}$ are observed close to the location of deep water upwelling in the PAZ. As these surface waters move equatorward, the additional nitrate consumption yields higher surface $\delta^{15}N_{nitrate}$ in the OAZ and SAZ, respectively.

The $\delta^{15}N$ of subsurface nitrate is primarily controlled by the isotope effects of denitrification and N_2 fixation, the processes that also determine the global ocean nitrate inventory (Sigman & Fripiat, 2019). Water column denitrification preferentially removes ^{14}N in oxygen deficient zones, leaving the residual nitrate enriched in ^{15}N (Cline & Kaplan, 1975), whereas N_2 fixation influences the global nitrate inventory via remineralization of

organic matter with a low $\delta^{15}N$ of ~ -1 ‰ (Carpenter et al., 1997; Hoering & Ford, 1960; Knapp et al., 2008). Because of additional controls on N_2 fixation and water column denitrification, these processes are not co-located within the oceans (Fig. 2), resulting in significant regional $\delta^{15}N_{nitrate}$ deviations. Specifically, the regional dominance of N_2 fixation lowers subsurface $\delta^{15}N_{nitrate}$ in the NASTG (Marconi et al., 2015), while water column denitrification raises subsurface $\delta^{15}N_{nitrate}$ in the ETSP and CTSP (Peters et al., 2018) (Fig. 3c). Benthic denitrification has a weak isotope effect relative to water column denitrification (Brandes & Devol; 2002; Lehmann et al., 2007), but it likely has an important indirect effect by stimulating additional N_2 fixation that delivers low $\delta^{15}N$ to the ocean (Somes et al, 2013; Ren et al., 2017).

Where nitrate is not completely consumed at the surface, the degree of nitrate utilization plays an important role in determining the $\delta^{15}N$ of sinking organic matter. For example, in regions of incomplete nitrate consumption, the $\delta^{15}N$ of sinking organic matter (that determining the exported $\delta^{15}N$, see below) should scale with the degree of nitrate consumption (f; Eq. 4-5). This link between nitrate assimilated in the surface ocean and export has been demonstrated using $\delta^{15}N$ of nitrate and sinking organic matter (Fawcett et al., 2011). This link allows for, in theory, quantitative reconstructions of past nitrate utilization using the sedimentary record of sinking organic matter $\delta^{15}N$, provided the $\delta^{15}N$ of subsurface nitrate supply is known. Note, however, that in areas of complete nitrate consumption, sinking organic matter $\delta^{15}N$ should equal the source nitrate $\delta^{15}N$. In these oligotrophic areas, sinking organic matter $\delta^{15}N$ does not record relative nitrate utilization, and instead informs on the $\delta^{15}N$ of subsurface nitrate supply to the surface ocean.

5.3 $\delta^{15}N$ Archives

Bulk sediments are an attractive archive for reconstructing past sinking organic matter $\delta^{15}N$ given the relative ease of measurement via elemental analyzer-isotope ratio mass spectrometry. However, bulk sediment $\delta^{15}N$ may be modified from sinking $\delta^{15}N$ by addition of non-marine organic matter and potential isotopic alteration by microbial degradation in the sediments (Robinson et al., 2012). In response to this potentially, and in some cases demonstrably altered or contaminated bulk sediment organic matter $\delta^{15}N$ archive (Martínez-García et al., 2014; Ren et al., 2009; Robinson et al., 2012; Straub et al., 2013), several new proxy methods have been developed to isolate the $\delta^{15}N$ of sinking organic matter in the sediments. These include compound-specific $\delta^{15}N$ measurements on compounds derived

from surface ocean productivity (porphyrins, Higgins et al., 2009), on organic matter bound within biominerals produced in the upper ocean (e.g. diatoms, radiolaria and planktic foraminifera, Horn et al., 2011a; Martínez-García et al., 2014; Ren et al., 2009; Ren et al., 2012; Robinson et al., 2005, 2015; Sigman et al., 1999; Studer et al., 2015; Smart et al., 2018, 2020), and on biominerals produced in the deep ocean via organisms that feed on sinking organic matter (deep-sea corals, Wang et al., 2014, 2017). These archives are more resistant to diagenesis and less prone to bias from allochthonous N input, but also come with their own complexities—including more intensive preparatory chemistry, sample limitation, and potential differences in species' internal N cycling (e.g., Smart et al., 2018).

5.4 Sources of uncertainty

Using $\delta^{15}N$ measurements in sedimentary archives to reconstruct past nitrate utilization requires that changes in the subsurface and any other source nitrate $\delta^{15}N$ are quantified or assumed constant, and that the supply of nitrate to the surface layer has also not changed over time. Nitrogen fixation and denitrification processes often dominate the $\delta^{15}N$ signal in tropical sedimentary records, complicating quantitative interpretation of utilization and its link to NEP. To reconstruct past changes in nitrate consumption, authors have begun using multiple sediment $\delta^{15}N$ records to quantify both the source nitrate $\delta^{15}N$ signal and the mixed isotopic signal, with varying degrees of success (Galbraith et al., 2008; Robinson et al., 2009; Rafter & Charles, 2012). Models with ^{15}N implemented as a tracer can estimate changes to nitrogen cycling on the local and global scale and provide another approach for separating source from utilization isotopic signatures on sediment $\delta^{15}N$ (Galbraith et al., 2013; Eugster et al., 2013; Somes et al., 2017).

For fossil-bound approaches, uncertainties in species' internal N cycles can be addressed with downcore records of $\delta^{15}N$ in multiple species. These generally show consistent $\delta^{15}N$ offsets between different foraminifera species over time at a given location, although more research is needed to understand the cause of these species offsets (Ren et al., 2009; 2015; 2017; Straub et al., 2013). More challenging is the separation of individual diatom species (Studer et al., 2015) and diatoms from other silicifiers, which may have starkly different $\delta^{15}N$ (Ren et al., 2015; Robinson et al., 2015). An additional complication is the potential feeding of zooplankton (including foraminifera) on particulate organic nitrogen

derived from recycled N, which may seasonally decouple fossil-bound $\delta^{15}N$ from the $\delta^{15}N$ of newly supplied nitrate in certain oceanographic regions (Smart et al., 2020).

6 Silicon isotopes

Dissolved silicon (dSi, principally in the form of orthosilicic acid) is an essential nutrient for the large number of marine organisms, known as silicifiers, that produce biogenic silica (bSi) for their skeletal/architectural structures. Silicon is present as three stable isotopes: ^{28}Si, ^{29}Si, and ^{30}Si, and deviations in the natural abundance ratios of these isotopes can reveal information regarding the chemical and biological processes active within oceanic systems (Sutton et al., 2018).

6.1 Modern ocean dSi and $\delta^{30}Si$ of dSi distribution

The global mean dissolved silicon isotopic composition (denoted by $\delta^{30}Si$) of modern seawater depends on the flux and isotopic composition of the known inputs - rivers and glaciers, groundwater, hydrothermal activity, sedimentary processes and atmospheric dust - and outputs, namely reverse weathering and burial of bSi (Sutton et al., 2018). Changes in the mass balance of the different inputs, and end-member compositions of the constituents, are likely to cause changes in the budget of dSi and $\delta^{30}Si$ in the oceans through time, especially over timescales longer than the residence time of silicon in the oceans (~ 12 kyr; Frings et al., 2016). The geographical variation in dSi and $\delta^{30}Si$ in modern oceanic waters is largely driven by biological uptake and remineralization of bSi, as well as large-scale oceanic circulation and mesoscale mixing processes. As with nitrogen isotopes, $\delta^{30}Si$ of dSi in surface Southern Ocean waters increases from the PAZ to OAZ and SAZ (Fig. 3d). This reflects preferential incorporation of isotopically light Si into bSi and resultant isotopic enrichment of the remaining dSi in surface waters, with greater dSi drawdown relative to supply in the SAZ, and progressively less utilization in the OAZ and PAZ, respectively (Cardinal et al., 2005; Fripiat et al., 2012). NASTG dSi $\delta^{30}Si$ is elevated at depth over the Southern Ocean (Fig. 3d), indicating the influence of overturning circulation on propagating isotopically enriched dSi

from the Arctic Ocean and isotopically depleted dSi from the Southern Ocean (Brzezinski & Jones, 2015).

6.2 Driving processes

Silicon uptake by membrane transporters and silicification are both widespread in eukaryotes and bacteria (Marron et al., 2016), although silica production in marine waters is dominated by diatoms. Silicifiers preferentially take up the lighter isotopes of silicon during biomineralization. As such, significant depletion or utilization of dSi by diatoms in surface waters results in progressive distillation of dSi, imparting an isotopic enrichment to the remaining dSi and the characteristic depth profile shown in Fig. 3d (see also Fig. 2). This distillation can be modelled as a Rayleigh-type closed process or a steady-state open system (Eq. 4 and 5, respectively), assuming a known starting δ^{30}Si of dSi value and a constant biological isotopic fractionation (De La Rocha et al., 1997; Varela et al., 2004). These equations rely on a number of challenging assumptions, regarding the nature of fractionation by different silicifiers, a unique, well-characterized dSi source, and the environmental controls on isotopic uptake during growth (Sutton et al., 2018).

6.3 Sedimentary archives for δ^{30}Si

The use of Si stable isotopes as a paleoceanographic proxy was established in the late 1990s based on its similarities to N and C isotope systems (De La Rocha et al., 1997, 1998). Initially, the influence of potentially confounding factors to this proxy, such as a variable isotopic fractionation (i.e. due to temperature), other planktic consumers of dSi (e.g. radiolaria and silicoflagellates) and the influence of dissolution on Si isotopic fractionation, were found to have a negligible effect or were not even considered. Since the late 1990's, experimental studies have highlighted potential biases concerning the usefulness of this proxy (Demarest et al., 2009; Sutton et al., 2013) that continue to be debated. The seasonal evolution of biogenic opal δ^{30}Si exported into deep sediment traps (Varela et al., 2004; Closset et al., 2015), the good agreement found between core tops and their mixed layer diatom counterparts (Egan et al., 2012), and the lack of a noticeable isotopic change during dissolution either in sediments (Wetzel et al., 2014) or in deep settling diatoms (Fripiat et al., 2012) confirm the rationale behind the use of the proxy. Similar to N and C isotopes, a change in the quantity of Si supplied and/or the source isotopic composition can influence the δ^{30}Si of diatoms in the sediment archives (recently highlighted by the very low δ^{30}Si of <0 ‰

for *Ethmodiscus rex,* Xiong et al., 2015), and should be considered when interpreting their geochemistry for paleoceanographic reconstructions. The δ^{30}Si of siliceous marine sponges is strikingly correlated to dSi concentration (Hendry et al. 2010; Wille et al., 2010) and provides a paleo-proxy of the dSi supply to the mixed layer, which can be used to better constrain diatom paleo-productivity. Thus, the δ^{30}Si of different silicifiers preserved in marine sediment cores, especially when combined with other sedimentary and geochemical archives (e.g. Ge/Si ratio, Shemesh et al., 1988), provides additional constraints on past changes of the silicon cycle over geological timescales.

6.4 Sources of uncertainty for paleoproductivity estimation

In addition to the previously discussed process-related biases, the use of δ^{30}Si as an *ad hoc* paleo-productivity proxy and its interpretation can also be influenced by differences in methodology and currently poorly constrained sources of error (e.g. diagenesis; Sutton et al., 2018). An important challenge for δ^{30}Si measurements and their interpretation in the paleo-records is ensuring that the biogenic opal is free of contaminating sources of Si (e.g. clay, authigenic Al-Si; Ehlert et al., 2016). Therefore, it is strongly suggested that all protocols used to clean bSi for δ^{30}Si measurement ensure frequent visual inspection of the samples (Sutton et al., 2018). In addition, it should be kept in mind that δ^{30}Si may reflect the productivity of silicifiers but not total productivity, as these two processes could be decoupled.

7 Applications

Carbon, nitrogen, and silicon isotopes have been vital for reconstructing nutrient utilization, the past biological pump, and changing ocean nutrient cycling over a range of timescales. Here we provide examples of such applications, focusing on Late Quaternary glacial-interglacial cycles and longer-term changes throughout the Cenozoic.

7.1 Late Quaternary glacial-interglacial cycles

Understanding glacial-interglacial variability in atmospheric pCO_2 is *cause célèbre* for geochemical paleoproductivity proxies. Discussed here are δ^{13}C, δ^{15}N, and δ^{30}Si proxy applications linking ocean productivity and atmospheric pCO_2 over the past 50,000 years (50 kyr). Many suitable reconstructions exist for this time interval; for the sake of brevity, only a

few example records are presented. Readers are encouraged to consult the references and recent reviews (Galbraith & Skinner, 2020; Hain et al., 2014; Hendry & Brzezinski, 2014; Sutton et al, 2018; Tesdal et al. 2013) for further discussion.

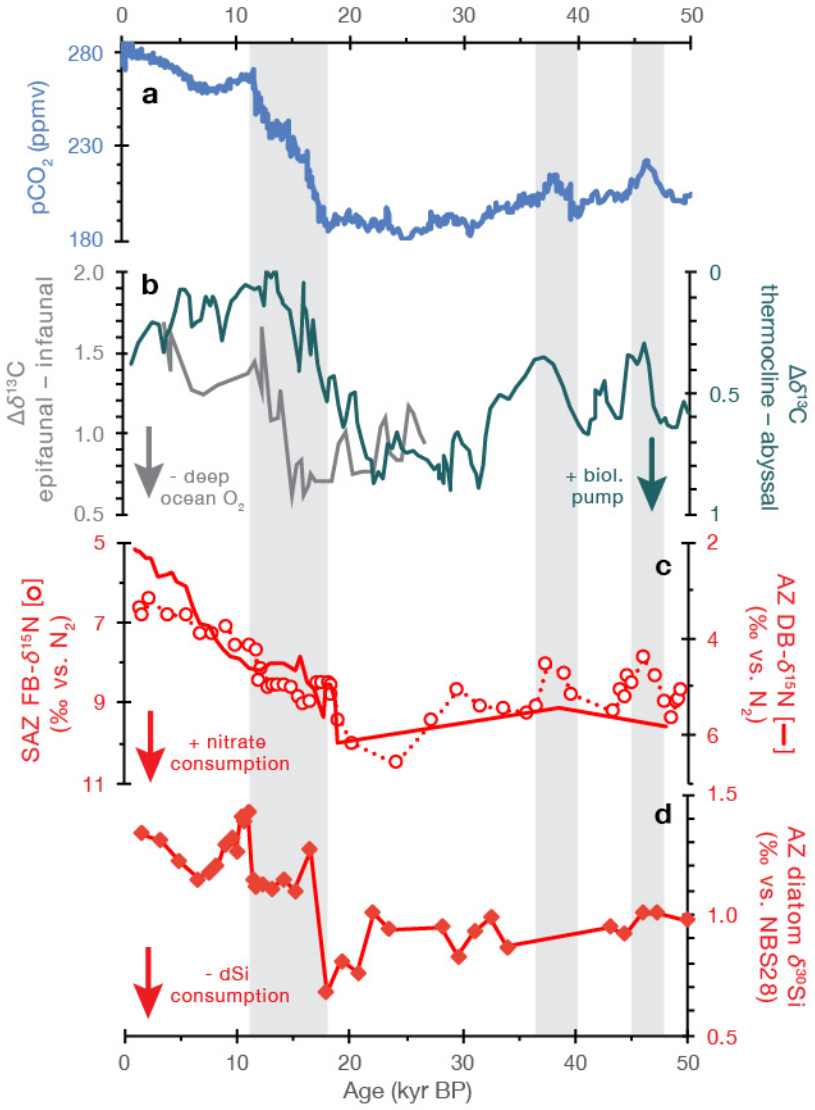

Figure 4. *Selected carbon, nitrogen, and silicon isotope records across the last glacial cycle. a) Atmospheric pCO_2 (Antarctic compilation from Monnin et al., 2004; MacFarling Meure et al., 2006; Bereiter et al., 2012; Rubino et al., 2013; Ahn & Brook, 2014; Marcott et al., 2014). b) Carbon isotope proxies for deep ocean oxygenation (gray, left axis; Hoogakker et al., 2018) and strength of the biological pump (teal, right axis; Ziegler et al., 2013). c) SAZ foraminifera-bound $\delta^{15}N$ (circles and dotted line, Martínez-García et al., 2014) and AZ diatom-bound $\delta^{15}N$ (Studer et al., 2015) indicating Southern Ocean nitrate consumption. d) Diatom $\delta^{30}Si$ indicating AZ dSi consumption (Robinson et al., 2014). Axes in b)-d) are oriented with up/down indicating a process change that tends to increase/decrease pCO_2. Vertical gray shading highlights geochemical proxy responses across three periods of increasing and/or elevated pCO_2.*

Atmospheric pCO_2 as reconstructed from a composite of Antarctic ice cores declines slightly from 50 to 20 ka with notable short-term pCO_2 maxima at Antarctic Isotope Maxima

(AIM) 12 (47 ka) and 8 (38 ka) (Fig. 4a) (Bereiter et al., 2012). Following the Last Glacial Maximum (LGM) pCO_2 minimum, pCO_2 shows a rapid, three-step increase during deglaciation from 18.1 ka to 11.1 ka (Marcott et al., 2014). Some sedimentary $\delta^{13}C$, $\delta^{15}N$, and $\delta^{30}Si$ records capture these pCO_2 features (Fig. 4b-d), indicating a connection between pCO_2 and past variations in aspects of ocean productivity. The link between these proxies and atmospheric pCO_2 indicates parallel changes in primary production, carbon export to the deep-sea, and respiration of organic carbon in the deep-sea—all processes associated with the biological carbon pump. Below, we examine sediment proxy records to highlight the utility of these geochemical tools and summarize understanding of the ocean's role in modulating glacial-interglacial atmospheric pCO_2 within the context of the Southern Ocean biological carbon pump and the Silicic Acid Leakage Hypothesis.

7.1.1 Southern Ocean biological carbon pump

Nitrogen isotopes of organic matter bound in planktic foraminifera (FB-$\delta^{15}N$) and diatoms (DB-$\delta^{15}N$) record past surface ocean nitrate consumption in the SAZ and AZ, respectively (Fig. 4c). Prior to the LGM, millennial-scale SAZ FB-$\delta^{15}N$ variations track pCO_2 (Fig. 4a) and dust flux, supporting changing iron fertilization of the SAZ and associated export production as a direct control on pCO_2 (Martínez-García et al., 2014). At the LGM, higher SAZ FB-$\delta^{15}N$ and AZ DB-$\delta^{15}N$ occur without evidence for changes in the $\delta^{15}N$ of mean ocean nitrate (Galbraith et al., 2013), implying more complete consumption of the nitrate supply to the surface Southern Ocean (Martínez-García et al., 2014; Studer et al., 2015). Since export production was higher in the SAZ and lower in the AZ compared to the late Holocene (Kohfeld et al., 2005; Jaccard et al., 2013), higher FB-$\delta^{15}N$ and DB-$\delta^{15}N$ argue for a more efficient SAZ biological pump and reduced nutrient supply to the surface AZ, respectively (Martínez-García et al., 2014; Studer et al., 2015). Both SAZ FB-$\delta^{15}N$ and AZ DB-$\delta^{15}N$ decline during the deglaciation, suggesting that SAZ and AZ nitrate utilization weakened coeval with increasing pCO_2. Intriguingly, AZ DB-$\delta^{15}N$ continues to decline throughout the Holocene, possibly contributing to the Holocene pCO_2 increase through outgassing of deep ocean CO_2 in the AZ (Studer et al., 2018).

Carbon isotope gradients between surface, intermediate, and bottom dwelling foraminifera have been used to reconstruct inferred changes in biological pump efficiency and its relationship to pCO_2 on glacial-interglacial timescales. Ziegler et al. (2013) used the $\delta^{13}C$ values of intermediate and bottom dwelling foraminifera to reconstruct the $\delta^{13}C$ gradient

between thermocline Subantarctic mode waters (SAMW) and abyssal circumpolar deep water (CDW) in the SAZ of the South Atlantic Ocean (Fig. 4b, teal curve). Prior to the LGM, substantial millennial-scale shifts in the $\delta^{13}C$ difference ($\Delta\delta^{13}C_{SAMW\text{-}CDW}$) have similar timing to changes in Antarctic ice core pCO_2 and dust flux records and SAZ FB-$\delta^{15}N$ (Fig. 4c; Martínez-García et al., 2014), as evident at AIM 8 and 12. The highest $\Delta\delta^{13}C_{SAMW\text{-}CDW}$ of the last 50 kyr occurs during the LGM, suggestive of an increased reservoir of carbon with a lower $\delta^{13}C$ in the deep Southern Ocean arising from a more efficient biological pump (Ziegler et al., 2013), which is also supported by a global model-data analysis of sedimentary $\delta^{13}C$ and $\delta^{15}N$ (Schmittner & Somes, 2016). This water mass $\delta^{13}C$ gradient breaks down during the deglaciation as $\Delta\delta^{13}C_{SAMW\text{-}CDW}$ decreases from 23 to 12 ka, overlapping with the deglacial pCO_2 rise. Additionally, Hertzberg et al. (2016) found a reduced $\delta^{13}C$ gradient between surface and intermediate depth foraminifera during two periods of deglacial atmospheric pCO_2 rise, suggesting a decrease in export production at these times.

The $\delta^{13}C$ difference between epifaunal and shallow infaunal benthic foraminifera ($\Delta\delta^{13}C_{E\text{-}I}$) has also been used to infer changes in bottom water oxygenation and carbon storage in the deep ocean on glacial-interglacial timescales. This carbon reservoir is thought to be a major source of carbon to the atmosphere on glacial-interglacial transitions via the Southern Ocean. Studies from the Atlantic (Gottschalk et al., 2016; Hoogakker et al., 2015, 2016) and Pacific oceans (Hoogakker et al., 2018; Umling & Thunell, 2018; Jacobel et al., 2020) utilized the $\Delta\delta^{13}C_{E\text{-}I}$ proxy to propose that the deep waters of these regions were important carbon storage sites during glacial periods. For instance, Hoogakker et al. (2018) showed lower $\Delta\delta^{13}C_{E\text{-}I}$ during the LGM in the equatorial Pacific, with a rapid $\Delta\delta^{13}C_{E\text{-}I}$ increase between 15 and 11 ka (Fig. 4b, gray curve). The $\Delta\delta^{13}C_{E\text{-}I}$ increase implies improving oxygenation of the deep Pacific and loss of respired carbon from the deep Pacific during the latter phase of deglacial pCO_2 rise. A cautionary note is that separating the effects of local changes in export production from changes in the more global signature of respiration and circulation on deep ocean $\delta^{13}C_{DIC}$ may not be trivial with these approaches.

7.1.2 Silicic Acid Leakage Hypothesis

Another potential mechanism to account for natural glacial-interglacial variability in pCO_2 is changes in the biological uptake of carbon by diatoms – relative to uptake by carbonate producing organisms – in the low latitudes (Brzezinski et al., 2002; Matsumoto et al., 2002; Matsumoto & Sarmiento, 2008). Increased dSi supply to low latitudes would tend

to favor diatom production over carbonate production, lowering pCO_2 by increasing the "rain ratio" of C_{org} to $CaCO_3$. The dSi supply to fuel this production has been proposed as originating from dust inputs (Harrison, 2000; Nozaki & Yamamoto, 2001), or "leakage" of intermediate waters with high dSi from the Southern Ocean (the Silicic Acid Leakage Hypothesis; Brzezinski et al., 2002; Matsumoto et al., 2002). This hypothesis relies on the observations that diatoms utilize major nutrients at a lower Si:N ratio under iron replete conditions (Hutchins & Bruland, 1998; Marchetti & Cassar, 2009), due to more silicification under limitation of photosynthesis (Claquin et al. 2002) or perhaps due to changes in assemblage (Closset et al., 2014).

At the LGM, diatom δ^{30}Si was lower in the SAZ (Beucher et al., 2007) and AZ (De La Rocha et al., 1998; Robinson et al., 2014) compared to the Holocene (Fig. 4d), nearly the opposite pattern from FB- and DB-δ^{15}N (Fig. 4c). These observations indicate that dSi utilization was lower relative to nitrate in Southern Ocean surface waters during the LGM. Coupling of diatom and sponge silicon isotope records confirms that dSi supply from upwelling outpaced dSi utilization during the LGM and early deglaciation (Fig. 4d) (Horn et al., 2011b; Robinson et al., 2014). This potentially allowed for the build-up of dSi in the surface Southern Ocean during the LGM, particularly in the Pacific Sector (Ellwood et al., 2010) which could then be transported with northward flowing water masses.

With regard to the Silicic Acid Leakage Hypothesis, the key test is whether unutilized Southern Ocean dSi was indeed exported to and utilized at low latitudes at the LGM. However, low latitude bSi accumulation rate records do not show a clear picture of higher diatom productivity at the LGM or over the deglaciation (Bradtmiller et al., 2006; Kienast et al., 2006; Richaud et al., 2007; Dubois et al., 2010; Calvo et al., 2011; Hayes et al., 2011; Pichevin et al., 2020). One record of diatom δ^{30}Si and DB-δ^{15}N from the eastern Equatorial Pacific indicates reduced dSi utilization relative to other nutrients during the LGM, although this most likely reflects changes in local levels of Fe stress (Pichevin et al., 2009). Moreover, sponge spicule δ^{30}Si records from low latitudes do not support a significant change in mode water dSi concentrations during the late glacial, except – again – in the case of the Pacific sector (Rousseau et al., 2016). Spicule δ^{30}Si records from the LGM onward instead highlight changes in low latitude dSi supply during abrupt climate events in the Atlantic (Hendry et al., 2012; 2016) and Pacific (Doering et al., 2016). These changes in low latitude dSi supply appear as a result of abrupt changes in ocean ventilation (the Silicic Acid Ventilation

Hypothesis, Hendry & Brzezinski, 2014) that occur during intervals of increasing pCO_2. In summary, while available data do not support the Silicic Acid Leakage Hypothesis mechanism for reduced glacial pCO_2, Late Quaternary changes in dSi supply and consumption may be an important consideration for the type and amount of biological productivity in different ocean regions.

7.2 Cenozoic

On Cenozoic timescales, $\delta^{13}C$, $\delta^{15}N$, and $\delta^{30}Si$ records from sediment archives are more difficult to interpret solely in terms of nutrient utilization or the biological pump. Large-scale changes in ocean/atmosphere circulation, tectonic events including gateway openings and closures, and variations in sources and sinks can influence records of element and isotope cycling over timescales greater than their residence times (e.g., changes in element inventories; see Fig. 2). Here, we provide an overview of Cenozoic isotopic variability that has been interpreted in the context of these various drivers.

Stable oxygen isotopes in benthic foraminifera reveal a gradual cooling of the Earth over the Cenozoic (Fig. 5a), superimposed with cyclic variability and sudden warming/cooling events (Zachos et al., 2001, 2008). The long-term Cenozoic $\delta^{13}C$ record derived from a global compilation of benthic foraminiferal $\delta^{13}C$ provides insight into the nature of global carbon cycle perturbations (Fig. 5b). On first order, $\delta^{13}C$ details changes in deep-sea circulation patterns that might trigger or arise from climate changes throughout the Cenozoic (Zachos et al., 2001). Climate warming (e.g., declining $\delta^{18}O$) during the Paleocene-Eocene Thermal Maximum (PETM, ~56 Ma) was associated with a massive carbon addition to the ocean-atmosphere system that led to a negative $\delta^{13}C$ excursion in marine carbonates

(Zachos et al., 2001). The source of this carbon is debated but has been linked most recently to volcanism associated with the North American Igneous Province (Gutjahr et al., 2017).

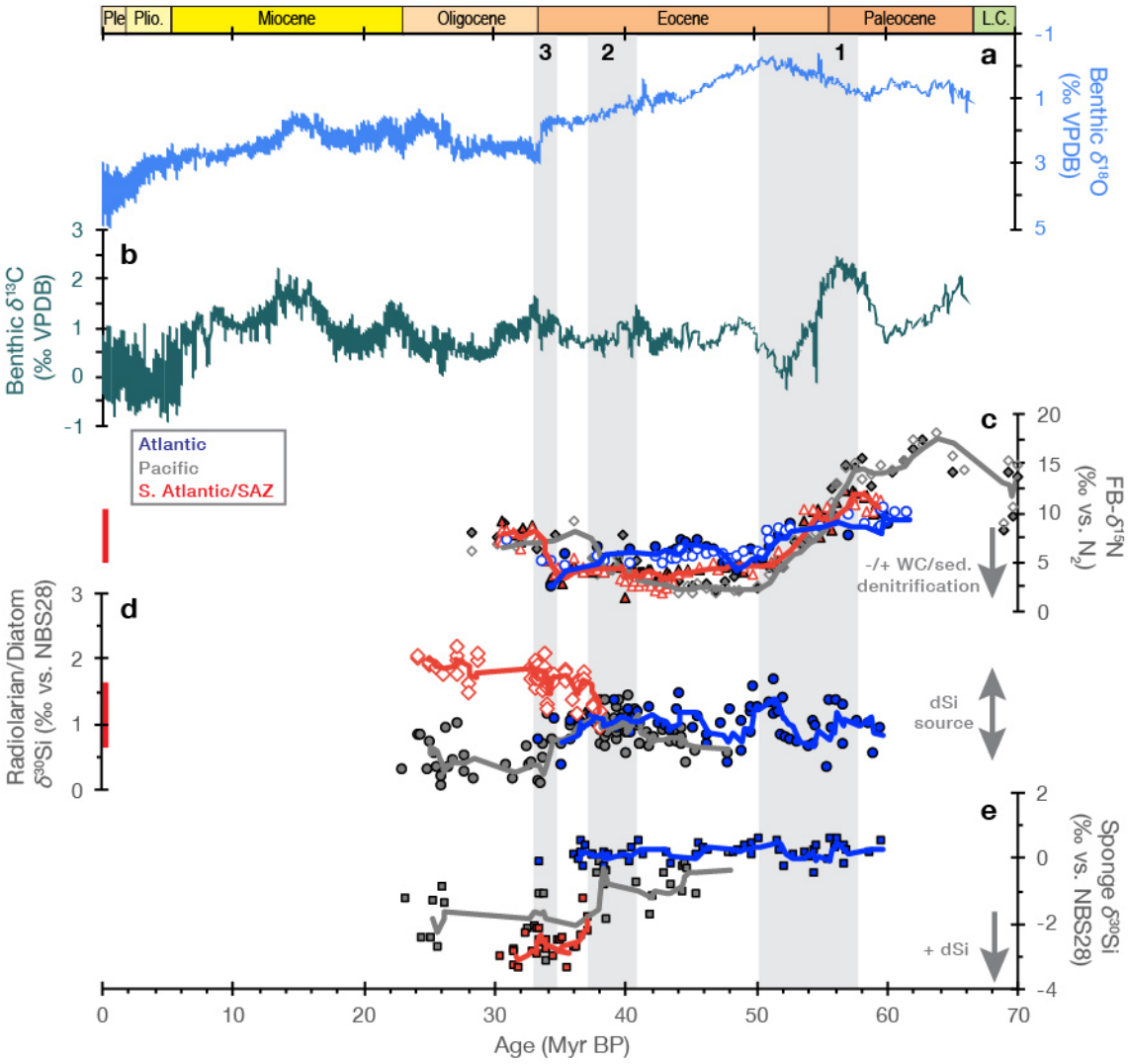

Figure 5. *Cenozoic climate and major element isotope variations (all isotope values in ‰ relative to accepted international standards). a) Global benthic foraminifera $\delta^{18}O$ and b) $\delta^{13}C$ (Zachos et al, 2001). c) Sponge $\delta^{30}Si$ indicating dSi concentration and d) Radiolarian (circles) and diatom (diamonds) $\delta^{30}Si$ indicating changing dSi sources (Egan et al., 2013; Fontorbe et al., 2016; 2017). e) Foraminifera-bound $\delta^{15}N$ indicating changes in the balance of water column (WC) and sedimentary (sed.) denitrification (Kast et al., 2019). Blue, gray, and red symbols in (c)-(e) indicate samples from Atlantic, Pacific, and South Atlantic/Subantarctic sediment cores (see individual studies for details). Red vertical lines in (c) and (d) denote the Late Quaternary ranges of Southern Ocean FB-$\delta^{15}N$ and diatom $\delta^{30}Si$ in Fig. 4. Vertical gray shading denotes three intervals of relevant climatic/tectonic change: (1) closure of the Tethys Sea; (2) formation of the Antarctic Circumpolar Current; (3) Eocene-Oligocene Transition. Time intervals of epochs indicated by colored boxes along top axis (after Walker et al., 2018); "L.C." is Late Cretaceous, "Plio." is Pliocene, and "Ple" is Pleistocene.*

The PETM punctuated a long term, ~2‰ $\delta^{13}C$ drop between 58 and 52 Ma that may indicate a decrease in organic carbon burial (Komar et al., 2013). During the Early Eocene Climatic Optimum (53 – 49 Ma), benthic foraminifera $\delta^{13}C$ increased by ~1‰ without a corresponding shift in benthic $\delta^{18}O$, possibly indicating a shift in the biological pump and/or ocean circulation under extreme greenhouse conditions (Laurentano et al., 2018). The growth of ice sheets during the Oligocene and Miocene (33.9 – 5.33 Ma) modulated climate at this time, with $\delta^{13}C$ and $\delta^{18}O$ covariance in the early Oligocene and middle Miocene attributed to changing ocean/atmosphere circulation, ocean productivity, and/or organic carbon burial (Zachos et al., 1997). On ~100 kyr timescales, negative excursions in $\delta^{13}C$ correspond with negative excursions in $\delta^{18}O$ for much of the Cenozoic, but this relationship flips after 5 Ma, with negative $\delta^{13}C$ excursions corresponding with positive $\delta^{18}O$ excursions for the Plio-Pleistocene. This switch may indicate a fundamental change in the relationship between climate and the carbon cycle during Plio-Pleistocene glaciations (Kirtland Turner, 2014).

FB-$\delta^{15}N$ indicates several intervals of profound alteration to the marine nitrogen cycle during the Cenozoic (Kast et al., 2019). Elevated Paleocene FB-$\delta^{15}N$ (Fig. 5c) suggests higher global mean ocean nitrate $\delta^{15}N$, reflecting an increased rate of global water column denitrification. This is possibly a result of greater production of low-oxygen intermediate depth waters from more extensive suboxia in the Paleocene ocean due to more widespread shallow seas (Kast et al., 2019). FB-$\delta^{15}N$ declined from 57-50 Ma in the early Eocene, coincident with the early stages of the Asia-India collision and the closure of the Tethys Sea. Low FB-$\delta^{15}N$ during the middle Eocene suggests that mean ocean nitrate $\delta^{15}N$ was lower than modern, a possible consequence of higher sedimentary denitrification fluxes caused by a greater area of submerged continental shelves during this period of elevated sea level (Kast et al., 2019). FB-$\delta^{15}N$ again increased around the Eocene-Oligocene transition at 35 Ma, implying a reduction in sedimentary denitrification associated with growth of the Antarctic ice sheets. The corresponding sea level fall would have exposed continental shelves and led to the loss of shelf-hosted sedimentary denitrification (Kast et al., 2019). Future records of nitrogen isotopes may provide higher resolution insights on the marine nitrogen cycle and productivity across key intervals of Earth's Cenozoic climate evolution.

The Cenozoic cooling trend coincided with a rapid diversification and expansion of diatoms, especially at the Eocene-Oligocene boundary and during the mid-Miocene, which may have led to a change in organic carbon burial and a drawdown of atmospheric pCO_2 (Finkel et al., 2005; Cermeño et al., 2015). Concentrations of dSi from the Paleocene onwards have been reconstructed using sponge spicule, radiolarian and diatom silicon

isotopes from marine sediment cores (Fig 5d-e). These proxy records suggest that from 60 to 30 Ma, dSi concentrations in the North Atlantic were uniformly low (Fig. 5e), possibly because diatoms (and other silicifiers) lowered global dSi in the early Cenozoic, if not before (Fontorbe et al., 2016; Conley et al., 2017). These records also suggest that Pacific deep waters experienced an increase in midwater dSi availability at approximately 37 Ma (Fig. 5e) as a result of ocean circulation shifts (Fontorbe et al., 2017), consistent with Southern Ocean silicon isotope archives that show the establishment of a proto-Antarctic Circumpolar Current and high-latitude upwelling at the Eocene-Oligocene boundary (Fig. 5d) (Egan et al., 2013).

8 Conclusions

Carbon, nitrogen, and silicon isotope ratios of marine sediments have served as principal geochemical tools over the last several decades for evaluating past surface ocean nutrient consumption and the strength of the biological pump. Despite their established use, the increasing spatiotemporal coverage of existing applications and the evolution of new sediment archives (e.g., sponge spicule δ^{30}Si and fossil-bound δ^{15}N) provide compelling new evidence for the covariation of regional nutrient utilization, the biological pump, and atmospheric pCO_2 over late Quaternary glacial cycles. On longer timescales, applications of C, N, and Si isotopes have shed light into the long-term drivers of ocean nutrient availability and connections between global nutrient and carbon cycles over the Cenozoic.

This review highlights two opportunities for future research. First, multiproxy applications are highly desirable given different impacts from ocean interface processes and internal ocean cycling on each isotope system (Fig. 2). Multiproxy applications benefit by both minimizing the potential bias of these non-productivity processes, and providing novel insights gained by concurrent inferences on the uptake of carbon and major nutrients. Promising examples include the co-application of diatom-bound N and diatom Si isotopes to Southern Ocean sediments to track variations between past nitrate and silicic acid limitation, and complementary insights on the efficiency of the biological pump from water column C isotope gradients and surface Subantarctic nutrient utilization from foraminifera-bound N isotopes. Second, the expansion of C, N and Si isotope proxies to the Cenozoic should greatly improve understanding of long-term C, N, and Si cycles. High-resolution applications of these tools to past Cenozoic climate events could improve knowledge of how ocean productivity affected, or was affected by, these events. Moreover, understanding patterns of ocean productivity in past warm climates may be of critical importance for a currently warming world that is on track to surpass any Late Quaternary climate analogue.

Acknowledgments, Samples, and Data

We thank the organizers, Bob Anderson, Catherine Jeandel, Kazuyo Tachikawa, and Laurence Vidal, and participants of the 2018 GEOTRACES-PAGES joint workshop on trace element and isotope proxies in paleoceanography, from which this manuscript developed. The authors thank Tim Conway for helpful feedback on a draft manuscript. This study was supported by the Past Global Changes (PAGES) project, which in turn received support from the Swiss Academy of Sciences and the US National Science Foundation. JRF acknowledges support from the Max Planck Society, the Tuttle Fund of the Department of Geosciences of Princeton University, the Grand Challenges Program of the Princeton Environmental Institute, and the Andlinger Center for Energy and the Environment of Princeton University.

Data availability statement: Datasets for this research are included in the papers (and their supplementary information files) referenced in Section 2.2: Brzezinski & Jones (2015); DeVries & Weber (2017); Fripiat et al. (2012; 2019); Marconi et al. (2015); Peters et al. (2018); and Schiltzer et al. (2018). New data were not created for this research.

GEOTRACES–PAGES Biological Productivity Working Group Members

C. Bolton (CEREGE, Univ. Aix-Marseille, CNRS, IRD, Collège de France, INRAE, Aix-en-Provence, France); E. Calvo (Institut de Ciències del Mar, CSIC, Barcelona, Spain); T. de Gadriel-Thoron (CEREGE, Univ. Aix-Marseille, CNRS, IRD, Collège de France, INRAE Aix-en-Provence, France); S. J. G. Galer (Max Planck Institute for Chemistry, Mainz, Germany); T. J. Horner (NIRVANA Labs & Department of Marine Chemistry & Geochemistry, Woods Hole Oceanographic Institution, Woods Hole, MA USA); F. Lacan (LEGOS, University of Toulouse, CNRS, CNES, IRD, UPS, Toulouse, France); S. H. Little (Department of Earth Sciences, University College London, London, UK); A. J. Lough (National Oceanography Centre, University of Southampton, Southampton, UK; now at School of Geography, Univeristy of Leeds, Leeds, UK); A. Tessin (Department of Geology, Kent State University, Kent, OH USA): A. Torfstein (Institute of Earth Sciences, Hebrew University, Jerusalem, & InterUniversity Institute for Marine Sciences, Eilat, Israel); G. Winckler (Lamont-Doherty Earth Observatory of Columbia University, Palisades, NY, USA); K. Wuttig (Antarctic Climate and Ecosystems Cooperative Research Centre, University of Tasmania, Hobart, Australia)

References

Ahn, J., & Brook, E. J. (2014). Siple Dome ice reveals two modes of millennial CO_2 change during the last ice age. *Nat. Commun.,* **5**, 3723, doi:10.1038/ncomms4723.

Altabet, M. A., & Francois, R. (1994). Sedimentary nitrogen isotopic ratio as a recorder for surface ocean nitrate utilization. *Global Biogeochem. Cycles*, **8**(1), 103–116.

Bauska, T., Joos, F., Mix, A., Roth, R., Ahn, J., & Brook, E. J. (2015). Links between atmospheric carbon dioxide, the land carbon reservoir and climate over the past millennium. *Nat. Geosci.,* **8**, 383–387.

Bereiter, B., Lüthi, D., Siegrist, M., Schüpbach, S., Stocker, T. F., & Fischer, H. (2012). Mode change of millennial CO_2 variability during the last glacial cycle associated with a bipolar marine carbon seesaw. *Proc. Natl. Acad. Sci.,* **109**, 9755-9760.

Berger, W. H., Smetacek, V., & Wefer, G. (1989). Ocean productivity and paleoproductivity - an overview. In W. H. Berger, V. S. Smetacek, G. Wefer (Eds) *Productivity of the Oceans present and past: Report of the Dahlem Workshop on Productivity of the Ocean, Berlin, 1988*, Life Sciences Research Reports 44, Wiley & Sons, Chichester, pp. 1-34.

Beucher, C. P., Brzezinski, M. A., & Crosta, X. (2007). Silicic acid dynamics in the glacial sub-Antarctic: Implications for the silicic acid leakage hypothesis. *Global Biogeochem. Cycles*, **21**, GB3015, doi:10.1029/2006GB002746.

Bradtmiller, L. I., Anderson, R. F., Fleisher, M. Q., & Burckle, L. H. (2006). Diatom productivity in the equatorial Pacific Ocean from the last glacial period to the present: a test of the silicic acid leakage hypothesis. *Paleoceanography*, **21**, PA4201, doi:10.1029/2006PA001282.

Brandes, J. A., & Devol, A. H. (2002). A global marine fixed nitrogen isotopic budget: Implications for Holocene nitrogen cycling. *Global Biogeochem. Cycles,* **16**, 1120, doi:10.1029/2001GB001856.

Broecker, W.S. (1982). Glacial to interglacial changes in ocean chemistry. *Prog. Oceanogr.* **11**, 151-197.

Broecker, W.S., & Maier-Reimer, E. (1992). The influence of air and sea exchange on the carbon isotope distribution in the sea. *Global Biogeochem. Cycles* **6**, 315-320.

Broecker, W.S., & Peng, T.H. (1982). Tracers in the Sea. Eldigio, Palisades, New York.

Brzezinski, M. A., & Jones, J. L. (2015). Coupling of the distribution of silicon isotopes to the meridional overturning circulation of the North Atlantic Ocean. *Deep Sea Res. Pt II*, **116**, 79–88. doi:10.1016/j.dsr2.2014.11.015

Brzezinski, M. A., Sigman, D. M., Sarmiento, J. L., Matsumoto, K., Gruber, N., Rau, G. H., & Coale, K. H. (2002). A switch from $Si(OH)_4$ to NO_3^- depletion in the glacial Southern Ocean. *Geophys. Res. Lett.*, **29**, 1564, doi:10.1029/2001GL014349.

Calvo, E., Pelejero, C., Pena, L. D., Cacho, I., & Logan, G. A. (2011). Eastern Equatorial Pacific productivity and related-CO_2 changes since the last glacial maximum. *Proc. Natl. Acad. Sci.,* **108**, 5537-5541, doi:10.1073/pnas.1009761108.

Cardinal, D., Alleman, L. Y., Dehairs, F., Savoye, N., Trull, T. W., & André, L. (2005). Relevance of silicon isotopes to Si-nutrient utilization and Si-source assessment in Antarctic waters. *Global Biogeochem. Cycles*, **19**(2), GB2007, doi:10.1029/2004GB002364.

Carpenter, E. J., Harvey, H. R., Fry, B., & Capone, D. G. (1997). Biogeochemical tracers of the marine cyanobacterium *Trichodesmium*. *Deep Sea Res. Pt. I*, **44**, 27-38.

Cermeño, P., Falkowski, P. G., Romero, O. E., Schaller, M. F., & Vallina, S. M. (2015). Continental erosion and the Cenozoic rise of marine diatoms. *Proc. Natl. Acad. Sci.*, **112**(14), 4239-4244.

Claquin, P., Martin-Jezequel, V., Kromkamp, J. C., Veldhuis, M. J. W., & Kraay, G. W. (2002). Uncoupling of silicon compared with carbon and nitrogen metabolisms and the role of the cell cycle in continuous cultures of *Thalassiosira pseudonana* (Bacillariophycae) under light, nitrigen and phosphorus control. *Journal of Phycology*, **38**(5), 922–930. http://doi.org/10.1046/j.1529-8817.2002.t01-1-01220.x

Cline, J. D., & Kaplan, I. R. (1975). Isotopic fractionation of dissolved nitrate during denitrification in the eastern tropical North Pacific Ocean. *Mar. Chem.* **3**, 271-299.

Closset, I., Lasbleiz, M., Leblanc, K., Quéguiner, B., Cavagna, A.-J., Elskens, M., et al. (2014). Seasonal evolution of net and regenerated silica production around a natural Fe-fertilized area in the Southern Ocean estimated with Si isotopic approaches. *Biogeosciences*, **11**(20), 5827–5846.

Closset, I., Cardinal, D., Bray, S. G., Thil, F., Djouraev, I., Rigual-Hernández, A. S., & Trull, T. W. (2015). Seasonal variations, origin, and fate of settling diatoms in the Southern Ocean tracked by silicon isotope records in deep sediment traps. *Global Biogeochem. Cycles*, **29**(9), 1495–1510. http://doi.org/10.1002/2015GB005180.

Conley, D. J., Frings, P. J., Fontorbe, G., Clymans, W., Stadmark, J., Hendry, K. R., et al. (2017). Biosilicification drives a decline of dissolved Si in the oceans through geologic time. *Front. Mar. Sci.*, **4**, 397, doi.org/10.3389/fmars.2017.00397.

Costa, K. M., Hayes, C. M., Anderson, R. F., Pavia, F. J., Bausch, A., Deng, F., et al. (2020). ^{230}Th normalization: New insights on an essential tool for quantifying sedimentary fluxes in the modern and Quaternary ocean. *Paleoceanography and Paleoclimatology*, **35**, doi:10.1029/2019PA003820.

Curry, W. B., & Oppo, D. W. (2005). Glacial water mass geometry and the distribution of $\delta^{13}C$ of ΣCO_2 in the western Atlantic Ocean. *Paleoceanography,* **20**, PA1017.

De La Rocha, C. L., Brzezinski, M. A., & DeNiro, M. J. (1997). Fractionation of silicon isotopes by marine diatoms during biogenic silica formation. *Geochim. Cosmochim. Acta*, **61**(23), 5051–5056.

De La Rocha, C., Brzezinski, M. A., DeNiro, M. J., & Shemesh, A. (1998). Silicon isotope composition of diatoms as an indicator of past oceanic change. *Nature*, **395**, 680-683.

Demarest, M. S., Brzezinski, M. A., & Beucher, C. P. (2009). Fractionation of silicon isotopes during biogenic silica dissolution. *Geochim. Cosmochim. Acta*, **73**(19), 5572–5583. http://doi.org/10.1016/j.gca.2009.06.019

DeVries, T., & Weber, T. (2017). The export and fate of organic matter in the ocean: New constraints from combining satellite and oceanographic tracer observations, *Global Biogeochem. Cycles*, **31**, 535–555, doi:10.1002/2016GB005551.

Doering, K., Erdem, Z., Ehlert, C., Fleury, S., Frank, M., & Schneider, R. (2016). Changes in diatom productivity and upwelling intensity off Peru since the Last Glacial Maximum: Response to basin-scale atmospheric and oceanic forcing. *Paleoceanography*, **31**(10), 1453-1473.

Dubois, N., Kienast, M., Kienast, S., Calvert, S. E., Francois, R., & Anderson, R. F. (2010). Sedimentary opal records in the eastern equatorial Pacific: it's not all about leakage. *Global Biogeochem. Cycles*, **24**, GB4020, doi:10.1029/2010GC003821.

Dugdale, R. C., & Goering, J. J. (1967). Uptake of new and regenerated forms of nitrogen in primary production. *Limnol. Oceanogr.*, **12**(2), 196–206.

Egan, K. E., Rickaby, R. E. M., Leng, M. J., Hendry, K. R., Hermoso, M., Sloane, H. J., et al. (2012). Diatom Silicon Isotopes as a Proxy for Silicic Acid Utilisation: a Southern Ocean Core Top Calibration. *Geochim. Cosmochim. Acta*, **96**, 174-192. http://doi.org/10.1016/j.gca.2012.08.002.

Egan, K. E., Rickaby, R. E. M., Hendry, K. R., & Halliday, A. N. (2013). Opening the gateways for diatoms primes Earth for Antarctic glaciation. *Earth Planet. Sci. Lett.*, **375**, 34–43. doi:10.1016/j.epsl.2013.04.030.

Ehlert, C., Doering, K., Wallmann, K., Scholz, F., Sommer, S., Grasse, P., et al. (2016). Stable silicon isotope signatures of marine pore waters – Biogenic opal dissolution versus authigenic clay mineral formation. *Geochim. Cosmochim. Acta*, **191**, 102–117. https://doi.org/10.1016/j.gca.2016.07.022.

Eide, M., Olsen, A., Ninnemann, U. S., & Eldevik, T. (2017). A global estimate of the full oceanic ^{13}C Suess effect since the preindustrial. *Global Biogeochem. Cycles*, **31**, 492–514.

Ellwood, M. J., Wille, M., & Maher, W. (2010). Glacial Silicic Acid Concentrations in the Southern Ocean. *Science*, **330**, 1088-1091.

Eppley, R. W., & Peterson, B. J. (1979). Particulate organic matter flux and planktonic new production in the deep ocean. *Nature*, **282**(5740), 677–680.

Eugster, O., Gruber, N., Deutsch, C., Jaccard, S. L., & Payne, M. R. (2013). The dynamics of the marine nitrogen cycle across the last deglaciation. *Paleoceanography*, **28**, 116-129, doi:10.1002/palo.20020.

Fawcett, S. E., Lomas, M., Casey, J. R., Ward, B. B., & Sigman, D. M. (2011). Assimilation of upwelled nitrate by small eukaryotes in the Sargasso Sea. *Nat. Geosci.*, **4**(10), 717–722. https://doi.org/10.1038/ngeo1265.

Felix, M. (2014). A comparison of equations commonly used to calculate organic carbon content and marine palaeoproductivity from sediment data. *Mar. Geol.,* **347**, 1-11.

Finkel, Z. V., Katz, M. E., Wright, J. D., Schofield, O. M., & Falkowski, P. G. (2005). Climatically driven macroevolutionary patterns in the size of marine diatoms over the Cenozoic. *Proc. Natl. Acad. Sci.*, **102**(25), 8927-8932.

Fontorbe, G., Frings, P. J., Christina, L., Hendry, K. R., & Conley, D. J. (2016). A silicon depleted North Atlantic since the Palaeogene: Evidence from sponge and radiolarian silicon isotopes. *Earth Planet. Sci. Lett.*, **453**, 67-77.

Fontorbe, G., Frings, P. J., De La Rocha, C. L., Hendry, K. R., Carstensen, J., & Conley, D. J. (2017). Enrichment of dissolved silica in the deep Equatorial Pacific during the Eocene-Oligocene. *Paleoceanography*, **32**(8), 848-863.

Frings, P. J., Clymans, W., Fontorbe, G., De La Rocha, C. L., & Conley, D. J. (2016). The continental Si cycle and its impact on the ocean Si isotope budget. *Chem. Geol.*, **425**, 12-36, doi:10.1016/j.chemgeo.2016.01.020.

Fripiat, F., Cavagna A.-J., Dehairs F., de Brauwere A., André L., & Cardinal D. (2012). Processes controlling the Si-isotopic composition in the Southern Ocean and application for paleoceanography. *Biogeosciences*, **9**, 2443–2457.

Fripiat, F., Martínez-García, A., Fawcett, S. E., Kemeny, P. C., Studer, A. S., Smart, S. M., et al. (2019). The isotope effect of nitrate assimilation in the Antarctic Zone: Improved estimates and paleoceanographic implications. *Geochim. Cosmochim. Acta,* **247**, 261-279, doi: 10.1016/j.gca.2018.12.003.

Galbraith, E. D., & Jaccard, S. L. (2015). Deglacial weakening of the oceanic soft tissue pump: global constraints from sedimentary nitrogen isotopes and oxygenation proxies. *Quat. Sci. Rev.,* **109**, 38-48.

Galbraith, E. D., & Skinner, L. C. (2020). The Biological Pump During the Last Glacial Maximum. *Annu. Rev. Mar. Sci.*, **12**, 559-586, doi:10.1146/annurev-marine-010419-010906.

Galbraith, E. D., Kienast, M., Jaccard, S. L., Pedersen, T. F., Brunelle, B. G., Sigman, D. M., & Kiefer, T. (2008). Consistent relationship between global climate and surface nitrate utilization in the western subarctic Pacific throughout the last 500 ka. *Paleoceanography*, **23**(2). https://doi.org/10.1029/2007pa001518.

Galbraith, E. D., Kienast, M., & NICOPP working group members (2013). The acceleration of oceanic denitrification during deglacial warming. *Nat. Geosci.,* **6**, 579-584.

Gottschalk, J., Skinner, L. C., Lippold, J., Vogel, H., Frank, N., Jaccard, S. L., & Waelbroeck, C. (2016). Biological and physical controls in the Southern Ocean on past millennial-scale atmospheric CO_2 changes. *Nat. Commun.,* **7**, 11539, doi:10.1038/ncomms11539.

Gutjahr, M., Ridgwell, A., Sexton, P. F., Anagnostou, E., Pearson, P. N., Pälike, H., Norris, R. D., Thomas, E., & Foster, G. L. (2017). Very large release of mostly volcanic carbon during the Palaeocene-Eocene Thermal Maximum. *Nature,* **548**, 573-577, doi:10.1038/nature23646.

Hain, M. P., Sigman, D. M., & Haug, G. H. (2014). The Biological Pump in the Past. In *Treatise on Geochemistry 2nd Edition*, Elsevier, 485-517.

Harrison, K. G. (2000). Role of increased marine silica input on paleo-pCO_2 levels. *Paleoceanography*, **15**, 292-298.

Hayes, C. T., Anderson, R. F., & Fleisher, M. Q. (2011). Opal accumulation rates in the equatorial Pacific and mechanisms of deglaciation. *Paleoceanography*, **26**, PA1207, doi:1210.1029/2010PA002008.

Hendry, K. R., & Brzezinski, M. A. (2014). Using silicon isotopes to understand the role of the Southern Ocean in modern and ancient biogeochemistry and climate. *Quat. Sci. Rev.*, **89**, 13-26.

Hendry, K. R., Leng, M. J., Robinson, L. F., Sloane, H. J., Blusztjan, J., Rickaby, R. E. M., Bastian Georg, R., & Halliday, A. N. (2010). Silicon isotopes in Antarctic sponges: an interlaboratory comparison. *Antarctic Science*, **23**(01), 34–42. http://doi.org/10.1017/S0954102010000593.

Hendry, K. R., Robinson, L. F., Meredith, M. P., Mulitza, S., Chiessi, C. M., & Arz, H. (2012). Abrupt changes in high-latitude nutrient supply to the Atlantic during the last glacial cycle. *Geology*, **40**(2), 123-126.

Hendry, K. R., Gong, X., Knorr, G., Pike, J., & Hall, I. R. (2016). Deglacial diatom production in the tropical North Atlantic driven by enhanced silicic acid supply. *Earth Planet. Sci. Lett.*, **438**, 122-129.

Hertzberg, J. E., Lund, D. C., Schmittner, A, & Skrivanek, L. (2016). Evidence for a biological pump driver of atmospheric CO_2 rise during Heinrich Stadial 1. *Geophys. Res. Lett.* **43**, 12242-12251.

Higgins, M. B., Robinson, R. S., Casciotti, K. L., McIlvin, M. R., & Pearson, A. (2009). A Method for Determining the Nitrogen Isotopic Composition of Porphyrins. *Anal. Chem.* **81** (1), 184-192, doi:10.1021/ac8017185.

Hoering, T. C., & Ford, H. T. (1960). The isotope effect in the fixation of nitrogen by *Azotobacter*. *J. Am. Chem. Soc.*, **82**, 376-378.

Hoogakker, B. A. A., Elderfield, H., Schmiedl, G., McCave, I. N., & Rickaby, R. E. M. (2015). Glacial-interglacial changes in bottom-water oxygen content on the Portuguese margin. *Nat. Geosci.* **8** (1), 40-43.

Hoogakker, B. A. A., Thornalley, D. J. R., & Barker, S. (2016). Millennial changes in North Atlantic oxygen concentrations. *Biogeosciences*, **13**, 211-221, doi:10.5194/bg-13-211-2016.

Hoogakker, B. A. A., Lu, Z., Umling, N., Jones, L., Zhou, X., Rickaby, R. E. M., Cartapanis, O., & Galbraith, E. D. (2018). Glacial expansion of oxygen-depleted seawater in the eastern tropical Pacific. *Nature* **242**, 240.

Horn, M. G., Robinson, R. S., Rynearson, T. A., & Sigman, D. M. (2011a). Nitrogen isotopic relationship between diatom-bound and bulk organic matter of cultured polar diatoms. *Paleoceanography*, **26**, PA3208, doi:10.1029/2010PA002080.

Horn, M. G., Beucher, C., Robinson, R. S., & Brzezinski, M. A. (2011b). Southern Ocean nitrogen and silicon dynamics during the last deglaciation. *Earth Planet. Sci. Lett.*, **310**, 334-339.

Horner T., Little, S. H., Conway, T. M., Farmer, J. R., Hertzberg, J. H. et al. Bioactive trace metals and their isotopes as paleoproductivity proxies: An assessment using GEOTRACES-era data. Submitted to *Global Biogeochem. Cycles.*

Hutchins, D. A., & Bruland, K. W. (1998). Iron-limited diatom growth and Si:N uptake ratios in a coastal upwelling regime. *Nature*, **393**, 65–68.

Jaccard, S. L., Hayes, C. T., Martínez-García, A., Hodell, D. A., Anderson, R. F., Sigman, D. M., & Haug, G. H. (2013). Two Modes of Change in Southern Ocean Productivity Over the Past Million Years. *Science*, **339**, 1419-1423, doi:10.1126/science.1227545.

Jacobel, A. W., Anderson, R. F., Jaccard, S. L., McManus, J. F., Pavia, F. J., & Winckler, G. (2020). Deep Pacific storage of respired carbon during the last ice age: Perspectives from bottom water oxygen reconstructions. *Quat. Sci. Rev.*, **230**, doi:10.1016/j.quascirev.2019.106065.

Kast, E. R., Stolper, D. A., Auderset, A., Higgins, J. A., Ren, H., Wang, X. T., et al. (2019). Nitrogen isotope evidence for expanded ocean suboxia in the early Cenozoic. *Science*, **364**, 386-389, doi:10.1126/science.aau5784.

Keeling, C. D. (1979). The Suess effect: ^{13}carbon-^{14}carbon interrelations. *Environ. Int.*, **2**(4–6), 229–300.

Keeling, R. F., Graven, H. D., Welp, L. R., Resplandy, L., Bi, J., Piper, S. C., et al. (2017). Trend in ^{13}C discrimination of land photosynthesis. *Proc. Natl. Acad. Sci.,* 201619240.

Kienast, S. S., Kienast, M., Jaccard, S. L., Calvert, S. E., & Francois, R. (2006). Testing the silica leakage hypothesis with sedimentary opal records from the eastern equatorial Pacific over the last 150 kyrs. *Geophys. Res. Lett.*, **33**, L15607, doi:15610.11029/12006GL026651.

Kirtland Turner, S. (2014). Pliocene switch in orbital-scale carbon cycle/climate dynamics. *Paleoceanography*, **29**, 1256-1266, doi:10.1002/2014PA002651.

Kohfeld, K. E., Le Quére, C., Harrison, S. P., & Anderson, R. F. (2005). Role of Marine Biology in Glacial-Interglacial CO_2 Cycles. *Science,* **308**, 74-78, doi:10.1126/science.1105375.

Komar, N., Zeebe, R. E., & Dickens, G. R. (2013). Understanding long-term carbon cycle trends: The late Paleocene through the early Eocene. *Paleoceanography*, **28**, 650-662, doi:10.1002/palo.20060.

Knapp, A. N., Difiore, P. J., Deutsch, C., Sigman, D. M., & Lipschultz, F. (2008). Nitrate isotopic composition between Bermuda and Puerto Rico: Implications for N2 fixation in the Atlantic Ocean. *Global Biogeochem. Cycles* **22**, GB3014.

Kroopnick, P. M. (1974). Correlations between ^{13}C and ΣCO_2 in surface waters and atmospheric CO_2. *Earth Planet. Sci. Lett.,* **22**, 397-403.

Kroopnick, P. M. (1985). The distribution of ^{13}C of ΣCO_2 in the world oceans. *Deep Sea Res. Pt. A,* **32**, 57-84.

Lehmann, M. F., Sigman, D. M., McCorkle, D. C., Granger, J., Hoffman, S., Cane, G., & Brunelle, B. G. (2007). The distribution of nitrate $^{15}N/^{14}N$ in marine sediments and the impact of benthic nitrogen loss on the isotopic composition of oceanic nitrate. *Geochim. Cosmochim. Acta*, **71**, 538405494, doi:10.1016/j.gca.2007.07.025.

Lynch-Stieglitz, J., Stocker, T. F., Broecker, W. S., & Fairbanks, R. G. (1995). The influence of air-sea exchange on the isotopic composition of oceanic carbon: Observations and modeling. *Global Biogeochem. Cycles* **9**, 653-665.

MacFarling Meure, C. Etheridge, D., Trudinger, C. Steele, P., Langenfelds, R., van Ommen, T., et al. (2006). Law Dome CO_2, CH_4 and N_2O ice core records extended to 2000 years BP. *Geophys. Res. Lett.,* **33**, L14810, doi:10.1029/2006GL026152.

Marchetti, A., & Cassar, N. (2009). Diatom elemental and morphological changes in response to iron limitation: a brief review with potential paleoceanographic applications. *Geobiology*, **7**, 419-431.

Marconi, D., Weigand, M. A., Rafter, P. A., McIlbin, M. R., Forbes, M., Casciotti, K. L., & Sigman, D. M. (2015). Nitrate isotope distributions on the US GEOTRACES North Atlantic cross-basin section: Signals of polar nitrate sources and low latitude nitrogen cycling. *Mar. Chem.*, **177**, 143-156, doi:10.1016/j.marchem.2015.06.007

Marcott, S. A., Bauska, T. K., Buizert, C., Steig, E. J., Rosen, J. L., Cuffey, K. M., et al. (2014). Centennial-scale changes in the global carbon cycle during the last deglaciation. *Nature,* **514**, 616-619.

Martínez-García, A., Sigman, D. M., Ren, H., Anderson, R. F., Straub, M., Hodell, D. A. et al. (2014). Iron fertilization of the Subantarctic Ocean during the last ice age. *Science*, **343**, 1347-1350, doi:10.1126/science.1246848.

Matsumoto, K., Sarmiento, J. L., & Brzezinski, M. A. (2002). Silicic acid leakage from the Southern Ocean: A possible explanation for glacial atmospheric pCO_2. *Global Biogeochem. Cycles,* **16**, 1031, doi:10.1029/2001GB001442.

Matsumoto, K., & Sarmiento, J. L. (2008). A corollary to the silicic acid leakage hypothesis. *Paleoceanography*, **23**, PA2203, doi:10.1029/2007PA001515.

McCorkle, D. C., Keigwin, L. D., Corliss, B. H., & Emerson, S. R. (1990). The influence of microhabitats on the carbon isotopic composition of deep-sea benthic foraminifera. *Paleoceanography* **5**(2), 161-185.

Mook, W. G., Bommerson, J. C., & Staverman, W. H. (1974). Carbon isotope fractionation between dissolved bicarbonate and gaseous carbon dioxide. *Earth Planet. Sci. Lett.* **22**, 169-176.

Monnin, E., Steig, E. J., Siegenthaler, U., Kawamura, K., Schwander, J., Stauffer, B., et al. (2004). Evidence for substantial accumulation rate variability in Antarctica during the Holocene, through synchronization of CO_2 in the Taylor Dome, Dome C and DML ice cores. *Earth Planet. Sci. Lett.*, **224**, 45-54.

Nozaki, Y., & Yamamoto, Y. (2001). Radium 228 based nitrate fluxes in the eastern Indian Ocean and the South China Sea and silica-induced "alkalinity pump" hypothesis. *Global Biogeochem. Cycles*, **15**, 555-567.

Olsen, A., & Ninnemann, U. (2010). Large $\delta^{13}C$ gradients in the preindustrial North Atlantic revealed. *Science*, **330**(6004), 658–659.

Paytan, A. (2009) Ocean Paleoproductivity. In: Gornitz V. (eds) *Encyclopedia of Paleoclimatology and Ancient Environments*. Encyclopedia of Earth Sciences Series, Springer, Dordrecht.

Peters, B. D., Lam, P. J., & Casciotti, K. L. (2018). Nitrogen and oxygen isotope measurements of nitrate along the US GEOTRACES Eastern Pacific Zonal Transect (GP16) yield insights into nitrate supply, remineralization, and water mass transport. *Mar. Chem.*, **201**, 137–150. doi:10.1016/j.marchem.2017.09.009

Pichevin, L. E., Reynolds, B. C., Ganeshram, R. S., Cacho, I., Pena, L., Keefe, K., & Ellam, R. M. (2009). Enhanced carbon pump inferred from relaxation of nutrient limitation in the glacial ocean. *Nature*, **459**, 1114-1117, doi:10.1038/nature08101.

Pichevin, L. E., Ganeshram, R. S., & Dumont, M. (2020). Deglacial Si remobilization from the deep-ocean reveals biogeochemical and physical controls on glacial atmospheric CO_2 levels. *Earth Planet. Sci. Lett.*, **543**, 116332, doi:10.1016/j.epsl.2020.116332.

Quay, P., & Wu, J. (2015). Impact of end-member mixing on depth distributions of $\delta^{13}C$, cadmium and nutrients in the N. Atlantic Ocean. *Deep Sea Res. Pt. II*, **116**, 107-116.

Rafter, P. A., & Charles, C. D. (2012). Pleistocene equatorial Pacific dynamics inferred from the zonal asymmetry in sedimentary nitrogen isotopes. *Paleoceanography*, **27**, https://doi.org/10.1029/2012pa002367.

Rafter, P. A., Bagnell, A., Marconi, D., & DeVries, T. (2019). Global trends in marine nitrate N isotopes from observations and a neural network-based climatology. *Biogeosciences*, **16**, 2617-2633, doi:10.5194/bg-16-2617-2019.

Ren, H., Sigman, D. M., Meckler, A. N., Plessen, B., Robinson, R. S., Rosenthal, Y., & Haug, G. H. (2009). Foraminiferal isotope evidence of reduced nitrogen fixation in the ice age Atlantic Ocean. *Science,* **323**, 244-248, doi:10.1126/science.1165787

Ren, H., Sigman, D. M., Thunell, R. C., & Prokopenko, M. G. (2012). Nitrogen isotopic composition of planktonic foraminifera from the modern ocean and recent sediments. *Limnol. Oceanogr.,* **57**(4), 1011-1024, doi:10.4319/lo.2012.57.4.1011

Ren, H., Studer, A. S., Serno, S., Sigman, D. M., Winckler, G., Anderson, R. F., et al. (2015). Glacial-to-interglacial changes in nitrate supply and consumption in the subarctic North Pacific from microfossil-bound N isotopes at two trophic levels. *Paleoceanography,* **30**, 1217-1232, doi:10.1002/2014PA002765.

Ren, H., Sigman, D. M., Martínez-García, A., Anderson, R. F., Chen, M.-T., Ravelo, A. C., et al. (2017). Impact of glacial/interglacial sea level change on the ocean nitrogen cycle. *Proc. Natl. Acad. Sci.,* **114**(33), E6759-E6766, doi:10.1073/pnas.1701315114.

Richaud, M., Loubere, P., Pichat, S., & Francois, R. (2007). Changes in opal flux and the rain ratio during the last 50,000 years in the equatorial Pacific. *Deep Sea Res. Pt. II*, **54**, 762-771.

Robinson, R. S., Sigman, D. M., DiFiore, P. J., Rohde, M. M., Mashiotta, T. A., & Lea, D. A. (2005). Diatom-bound $^{15}N/^{14}N$: New support for enhanced nutrient consumption in the ice age subantarctic. *Paleoceanography*, **20**, doi:10.1029/2004PA001114.

Robinson, R. S., Martinez, P., Pena, L. D., & Cacho, I. (2009). Nitrogen isotopic evidence for deglacial changes in nutrient supply in the eastern equatorial Pacific. *Paleoceanography*, **24**(4). https://doi.org/10.1029/2008pa001702.

Robinson, R. S., Kienast, M., Albuquerque, A. L., Altabet, M., Contreras, S., Holz, R. D., et al. (2012). A review of nitrogen isotopic alteration in marine sediments. *Paleoceanography*, **27**. https://doi.org/10.1029/2012pa002321.

Robinson, R. S., Brzezinski, M. A., Beucher, C. P., Horn, M. G., & Bedsole, P. (2014). The changing roles of iron and vertical mixing in regulating nitrogen and silicon cycling in the Southern Ocean over the last glacial cycle. *Paleoceanography*, 29, 1179-1195, doi:10.1002/2014PA002686.

Robinson, R. S., Moore, T. C., Erhardt, A. M., & Scher, H. D. (2015). Evidence for changes in subsurface circulation in the late Eocene equatorial Pacific from radiolarian-bound nitrogen isotope values. *Paleoceanography*, **30**, 912-922, doi:10.1002/2015PA002777

Rousseau, J., Ellwood, M. J., Bostock, H., & Neil, H. (2016). Estimates of late Quaternary mode and intermediate water silicic acid concentration in the Pacific Southern Ocean. *Earth Planet. Sci. Lett.*, **439**, 101-108.

Rubino, M., Etheridge, D. M., Trudinger, C. M., Allison, C. E., Battle, M. O., Langenfelds, R. L., et al. (2013). A revised 1000 year atmospheric $\delta^{13}C$-CO_2 record from Law Dome and South Pole, Antarctica. *J. Gephys. Res. Atmos.*, **118**, 8482-8499, doi:10.1002/jgrd.50668.

Schlitzer, R., et al. (2018). The GEOTRACES intermediate data product 2017. *Chem. Geol.*, **493**, 210-223.

Schmittner, A., & Somes, C. J. (2016). Complementary constraints from carbon (^{13}C) and nitrogen (^{15}N) isotopes on the glacial ocean's soft-tissue biological pump. *Paleoceanography*, **31**, 669-693, doi:10.1002/2015PA002905.

Schmittner, A., Gruber, N., Mix, A. C., Key, R. M., Tagliabue, A., & Westberry, T. K. (2013). Biology and air-sea gas exchange controls on the distribution of carbon isotope ratios ($\delta^{13}C$) in the ocean. *Biogeosciences* **10**, 5793-5816.

Shemesh, A., Mortlock, R. A., Smith, R. J., & Froelich, P. N. (1988). Determination of Ge/Si in marine siliceous microfossils: Separation, cleaning and dissolution of diatoms and radiolaria. *Mar. Chem.* **25**, 305-323.

Sigman, D. M., & Fripiat, F. (2019). Nitrogen isotopes in the ocean. In J. K. Cochran, J. H. Bokuniewicz, L. P. Yager (Eds.), *Encyclopedia of Ocean Sciences, 3rd Edition* (pp. 263-278). Oxford, UK: Elsevier.

Sigman, D. M., & Hain, M. P. (2012). The Biological Productivity of the Ocean: Section 1, *Nature Education Knowledge,* **3**(10): 21.

Sigman, D. M., Altabet, M. A., Francois, R., McCorkle, D. C., & Gaillard, J.-F. (1999). The isotopic composition of diatom-bound nitrogen in Southern Ocean sediments. *Paleoceanography,* **14**(2), 118-134.

Sigman, D. M., Altabet, M. A., McCorkle, D. C., Francois, R., & Fischer, G. (2000). The δ^{15}N of nitrate in the Southern Ocean: Nitrogen cycling and circulation in the ocean interior. *J. Geophys. Res. Oceans*, **105**(C8), 19599-19614.

Sigman, D. M., Hain, M. P., &. Haug, G. H. (2010). The polar ocean and glacial cycles in atmospheric CO_2 concentration, *Nature*, **466**, 47-55, doi:10.1038/nature09149

Smart, S. M., Ren, H., Fawcett, S. E., Schiebel, R., Conte, M., Rafter, P. A., et al. (2018). Ground-truthing the planktic foraminifer-bound nitrogen isotope paleo-proxy in the Sargasso Sea. *Geochim. Cosmochim. Acta,* **235**, 463-482, doi:10.1016/j.gca.2018.05.023

Smart, S. M., Fawcett, S. E., Ren, H., Schiebel, R., Tompkins, E. M., Martínez-García, A., et al. (2020). The nitrogen isotopic composition of tissue and shell-bound organic matter of planktic foraminifera in Southern Ocean surface waters. *Geochem. Geophys. Geosyst.,* **21**, e2019GC008440.

Spero, H. J. (1998). Life history and stable isotope geochemistry of planktonic foraminifera. In: *Isotope Paleobiology and Paleoecology*. Paleontol. Soc. Tuscaloosa, Alabama, 7-36.

Spero, H., Bijma, J., Lea, D., & Bemis, B. (1997). Effect of seawater carbonate concentration on foraminiferal carbon and oxygen isotopes. *Nature,* **390**, 497–500.

Spero, H. J., Mielke, K. M., Kalve, E. M., Lea, D. W., & Pak, D. K. (2003). Multispecies approach to reconstructing eastern equatorial Pacific thermocline hydrography during the past 360 kyr. *Paleoceanography* **18**(1), 1022, doi:10.1029/2002PA00814.

Shackleton, N. J., Hall, M. A., Line, J., & Cang, S. (1983). Carbon isotope data in core V19-30 confirm reduced carbon dioxide concentration in the ice age atmosphere. *Nature* **306**, 319-322.

Somes, C. J., Schmittner, A., Galbraith, E. D., Lehmann, M. F., Altabet, M. A., Montoya, J. P., et al. (2010). Simulating the global distribution of nitrogen isotopes in the ocean. *Global Biogeochem. Cycles,* **24**, GB4019, doi:10.1029/2009GB003767.

Somes, C. J., Oschlies, A., & Schmittner, A. (2013). Isotopic constraints on the pre-industrial oceanic nitrogen budget. *Biogeosciences,* **10**, 5889-5910, doi:10.5194/bg-10-5889-2013.

Somes, C. J., Schmittner, A., Muglia, J., & Oschlies, A. (2017). A three-dimensional model of the marine nitrogen cycle during the Last Glacial Maximum constrained by sedimentary isotopes. *Front. Mar. Sci.*, **4**, doi:10.3389/fmars.2017.00108.

Sutton, J. N., Varela, D. E., Brzezinski, M. A., & Beucher, C. P. (2013). Species-dependent silicon isotope fractionation by marine diatoms. *Geochim. Cosmochim. Acta*, **104**, 300–309. https://doi.org/10.1016/j.gca.2012.10.057

Sutton, J. N., André, L., Cardinal, D., Conley, D. J., de Souza, G. F., Dean, J., et al. (2018). A review of the stable isotope bio-geochemistry of the global silicon cycle and its

associated trace elements. *Frontiers in Earth Science*, **5**. https://doi.org/10.3389/feart.2017.00112

Studer, A. J., Sigman, D. M., Martínez-García, A., Benz, V., Winckler, G., Kuhn, G. et al. (2015). Antarctic Zone nutrient conditions during the last two glacial cycles. *Paleoceanography, 30*, 845-862, doi:10.1002/2014PA002745.

Studer, A. J., Sigman, D. M., Martínez-García, A., Thöle, L. M., Michel, E., Jaccard, S. L., et al. (2018). Increased nutrient supply to the Southern Ocean during the Holocene and its implications for the pre-industrial atmospheric CO_2 rise. *Nat. Geosci.*, **11**, 756-760, doi:10.1038/s41561-018-0191-8.

Tappan, H. (1968). Primary production, isotopes, extinctions and the atmosphere. *Paleogeogr. Paleoclimatol. Paleoecol.* **4**, 187-210.

Tesdal, J.-E., Galbraith, E. D., & Kienast, M. (2013). Nitrogen isotopes in bulk marine sediment: linking seafloor observations with subseafloor records. *Biogeosciences,* **10**, 101-118, doi:10.5194/bg-10-101-2013.

Tribovillard, N., Algeo, T. J., Lyons, T., & Riboulleau, A. (2006). Trace metals as paleoredox and paleoproductivity proxies: an update. *Chem. Geol.*, **232**, 12-32, doi:10.1016/j.chemgeo.2006.02.012.

Umling, N. E., & Thunell, R. C. (2018). Mid-depth respired carbon storage and oxygenation of the eastern equatorial Pacific over the last 25,000 years. *Quat. Sci. Rev.*, **189**, 43-56.

Varela, D. E., Pride, C. J., & Brzezinski, M. A. (2004). Biological fractionation of silicon isotopes in Southern Ocean surface waters. *Global Biogeochem. Cycles*, **18**, GB1047. http://doi.org/10.1029/2003GB002140.

Volk, T., & Hoffert, M. I. (1985). Ocean Carbon Pumps: Analysis of Relative Strengths and Efficiencies in Ocean-Driven Atmospheric CO_2 Changes. In E.T. Sundquist, W. S. Broecker (Eds.), *The Carbon Cycle and Atmospheric CO_2: Natural Variations Archean to Present*. Geophysical Monographic Series v. 32, 99-110, American Geophysical Union, Washington, DC.

Wang, X. T., Prokopenko, M. G., Sigman, D. M., Adkins, J. F., Robinson, L. F., Ren, H., et al. (2014). Isotopic composition of carbonate-bound organic nitrogen in deep-sea scleractinian corals: A new window into past biogeochemical change. *Earth Planet. Sci. Lett.,* **400***,* 243-250, doi:10.1016/j.epsl.2014.05.048.

Wang, X. T., Sigman, D. M., Prokopenko, M. G., Adkins, J. F., Robinson, L. F., Hines, S. K., et al. (2017). Deep-sea coral evidence for lower Southern Ocean surface nitrate concentrations during the last ice age. *Proc. Natl. Acad. Sci.,* **114**(13), 3352-3357, doi:10.1073/pnas.1615718114.

Waser, N. A. D., Harrison, P. J., Nielsen, B., Calvert, S. E., & Turpin, D. H. (1998). Nitrogen isotope fractionation during the uptake and assimilation of nitrate, nitrite, ammonium, and urea by a marine diatom. *Limnol. Oceanogr.*, **43**, 215-224.

Wetzel, F., de Souza, G. F., & Reynolds, B. C. (2014). What controls silicon isotope fractionation during dissolution of diatom opal? *Geochim. Cosmochim. Acta*, **131**, 128–137. http://doi.org/10.1016/j.gca.2014.01.028.

Wille, M., Sutton, J., Ellwood, M. J., Sambridge, M., Maher, W., Eggins, S., & Kelly, M. (2010). Silicon isotopic fractionation in marine sponges: A new model for

understanding silicon isotopic variations in sponges. *Earth Planet. Sci. Lett.*, **292**(3–4), 281–289. http://doi.org/10.1016/j.epsl.2010.01.036.

Woodruff, F., Savin, S., & Douglas, R.G. (1980). Biological fractionation of oxygen and carbon isotopes by recent benthic foraminifera. *Mar. Micropaleontol*. **5**, 3-11.

Xiong, Z., Li, T., Algeo, T., Doering, K., Frank, M., Brzezinski, M. A., et al. (2015). The silicon isotope composition of *Ethmodicus rex* laminated diatom mats from the tropical West Pacific: Implications for silicate cycling during the Last Glacial Maximum. *Paleoceanography*, **30**, 803-823, doi:10.1002/2015PA002793.

Zachos, J. C., Flower, B. P., & Paul, H. (1997). Orbitally paced climate oscillations across the Oligocene/Miocene boundary. *Nature*, **388**, 567-570.

Zachos, J. C., Pagani, M., Sloan, L., Thomas, E., & Billups, K. (2001). Trends, Rhythms, and Aberrations in Global Climate 65 Ma to Present. *Science*, **292**, 686-693, doi:10.1126/science.1059412.

Zachos, J. C., Dickens, G. R., & Zeebe, R. E. (2008). An early Cenozoic perspective on greenhouse warming and carbon-cycle dynamics. *Nature*, **451**, 279-283.

Zhang, J., Quay, P. D., & Wilbut, D. O. (1995). Carbon isotope fractionation during gas-water exchange and dissolution of CO_2. *Geochim. Cosmochim. Acta,* **59**, 107-114.

Ziegler, M., Diz, P., Hall, I. R., & Zahn, R. (2013). Millennial-scale changes in atmospheric CO_2 levels linked to the Southern Ocean carbon isotope gradient and dust flux. *Nat. Geosci.*, **6**, 457-461, doi:10.1038/ngeo1782.